Coastal Engineering 189 (2024) 104476

Contents lists available at ScienceDirect

Coastal Engineering

journal homepage: www.elsevier.com/locate/coastaleng

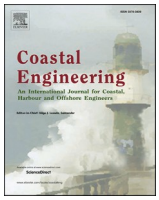

Small-scale field experiment on wave forces on a U-OWC breakwater

Alessandra Romolo *, Bruna Timpano, Valentina Laface, Vincenzo Fiamma, Felice Arena

Natural Ocean Engineering Laboratory NOEL, "Mediterranea" University of Reggio Calabria, Via Zehender - Loc. Feo di Vito, 89122 Reggio Calabria, Italy

ARTICLE INFO

Keywords:
Wave load
U-OWC breakwater
Wave pressure distribution
Small field experiment
Random sea waves
Probability of occurrence

ABSTRACT

A small-scale field experiment is conducted on a U-Oscillating Water Column (U-OWC) incorporated into a model of caisson breakwater at the Natural Ocean Engineering Laboratory (NOEL) laboratory of Reggio Calabria (Italy). The U-OWC or REWEC (REsonant Wave Energy Converter) is a device belonging to the family of Oscillating Water Columns (OWCs), characterized by the introduction of a U-duct. Such a device is innovative, absorbing a high percentage of incoming sea energy and, then, to produce electricity via a Power-Take-Off (PTO). The aim of the present study is the investigation of the wave pressures and forces acting on the U-OWC monolithic coastal defense structure. Moreover, the structural response of the U-OWC structure is also investigated under the occurrence of wave crests, by calculating the hydrodynamic forces realized in the active parts of the U-OWC. It is shown as a global additional force is realized, which contributes to increase the overall stability of the structure. Considering the wave loads acting on the U-OWC caisson, the post-process of the overall dataset recorded during the real field experiment at NOEL laboratory reveals the occurrence of both quasi-static loading (non-breaking), and of impact loading (impulsive) due to wave breaking. Thus, a systematic analysis is pursued in order to identify the loading cases acting on the U-OWC breakwater. When high non-breaking sea waves interact with the breakwater, "Quasi-Standing (QS)" wave pressures and forces occur at modified structure with two peaks of equal intensity. Instead, the impact of extreme breaking waves against the U-OWC structure generates asymmetrical wave pressure records beneath the wave crests, with two peaks with different intensity: the first one greater than the second one. In these cases, "Slightly Breaking (SB)" wave forces and "Impact Loads (IL)" are identified. Wave pressure distributions and forces acting on the U-OWC model are, then, investigated for the three classes of wave loads. Moreover, the probability of occurrence of maximum positive peak forces is determined from the experimental dataset, given a number of parameters. In particular, when QSWs occur, the maxima peak forces are recorded for deeper water depths d_n, d' and a, at given significant wave height H_{S_i}. Instead, for SBWs and ILs, the extreme wave loads are realized, when the most severe sea states occur with higher H_{S_i} , and for decreasing water depth d_n. d' and a. Then, the influence both of the length of the berm and of the width of the U-duct in the front structure is considered. When the dimensions of both structural elements is reduced, the maxima wave forces occur in a fixed recorded sea state. Then, the Quasi-Determinism (QD) nonlinear model at the U-OWC breakwater is introduced for evaluation of Quasi-Standing wave loads, showing a good agreement among analytical and experimental results. Finally, the Goda's model is applied to calculate the wave pressure distributions acting on the external walls of the U-OWC model. The theoretical results given by the Goda's formulae are compared with experimental data, overestimating experimental results for both QSWs and SBWs and, significantly, underestimating IL conditions.

1. Introduction

The main purpose for the construction of harbors, from the origin of such infrastructures, has been the need to protect areas of water, and land, from the wave action of the sea. In this perspective, the harbor structures, such as breakwaters and vertical sea walls, must be designed to withstand the most violent loads due to sea waves.

Considering the sea wave impacts on a vertical structure, they are strongly influenced by a large number of parameters that affect wave evolution on the approach to a wall. These are the seabed topography in front of the wall, the mean water depth at the wall and in its proximity, the front wall behavior of vertical structure, the three-dimensionality of

* Corresponding author.
E-mail addresses: aromolo@unirc.it (A. Romolo), bruna.timpano@unirc.it (B. Timpano), valentina.laface@unirc.it (V. Laface), vincenzo.fiamma@unirc.it (V. Fiamma), arena@unirc.it (F. Arena).

https://doi.org/10.1016/j.coastaleng.2024.104476
Received 19 October 2023; Received in revised form 17 December 2023; Accepted 23 January 2024
Available online 31 January 2024

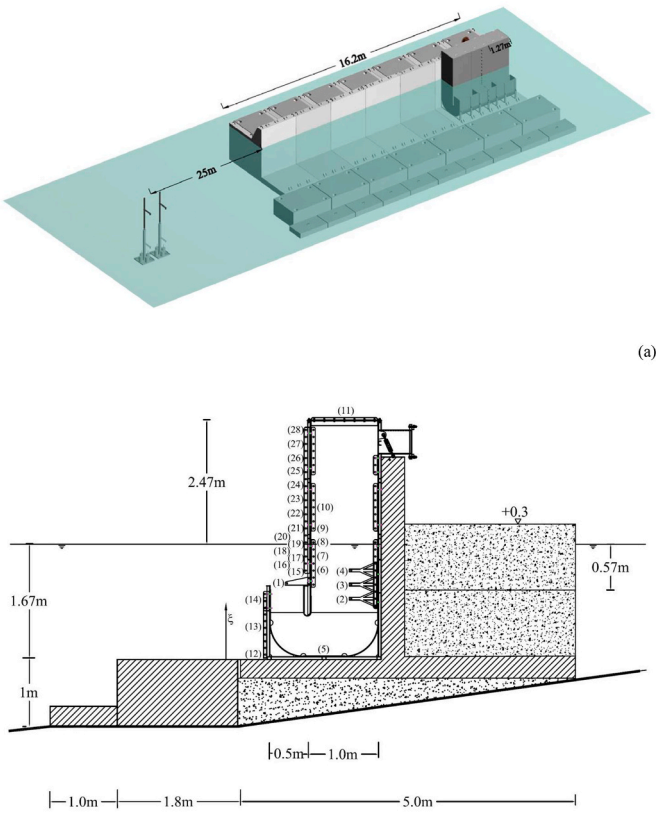

Fig. 1. (a) The site of the small-scale field experiment on the U-OWC breakwater at the Noel laboratory off the beach at Reggio Calabria (Italy - http://noel.unirc.it/); (b) The cross-section of the U-OWC integrated into a caisson breakwater and equipped with pressure transducers (1-28).

the sea waves and non-linear effects.

In the literature, depending on the behavior of the extreme wave impacts, the wave loads (pressure, pressure distribution, and total forces) on vertical breakwaters or seawalls have been classified as: *i*) "pulsating" wave loads, for which the expected response of the structure is "quasi-static", and the load durations are between approximately 0.2 and 0.5 times the incident wave period; *ii*) "impact" or "impulsive" loads, for which the load intensity is high, the load duration/time history is short with respect to the wave period (about 1/100), and they are relevant for the dynamic response of the structure (Oumeraci et al., 1993; Cuomo et al., 2010). In particular, impulsive loads are related to measured peak pressures exerted by a wave breaking against the sea wall.

In detail, quasi-steady forces (or pulsating forces) can be properly predicted by standard approaches based on inviscid, irrotational, and incompressible flow computations, while wave impulsive forces on seawalls can be much higher than quasi-steady forces and their occurrence involves complex impact mechanisms, such as breaking wave impact. In particular, the quasi-steady force is caused by slowly varied water motion, and can be accurately predicted by non-breaking standing waves, with linear and non-linear approaches (Goda, 2000; Boccotti, 2000, 2014; Romolo and Arena, 2008, 2013, Romolo et al., 2014). Instead, more complex methodologies based also on numerical and analytical methods (Cooker and Peregrine, 1995; Wood et al., 2000) or probabilistic approaches (Chen et al., 2019), have been developed in the last decades, to model the impulsive wave impact forces, which are affected by greater uncertainty.

In particular, a strong interest has been devoted to the evaluation of impulsive wave impact forces, due to their influence in the overall stability of vertical structures, and which have to be evaluated in addition to quasi-static wave forces. The qualitative and quantitative experimental determination of these impulsive forces has been examined widely, and it is based on field measurements (e.g., Bagnold, 1939; Kirkgoz, 1982; Oumeraci et al., 1993; Bullock et al., 2001; Peregrine, 2003; Cuomo et al., 2010; Boccotti et al., 2012), summarized on two substantial projects, Monlithic Coastal Structures (MCS) and PRObabilistic design tools for VERtical Breakwaters (PROVERBS), funded by the European Union's Marine Science and Technology (MAST) program (Oumeraci et al., 2001).

Moreover, nowadays sea wave energy is recognized as one of the most favourable sources of energy due to its abundance offshore as well as near-shore. A tendency of the market, due to their cost-effectiveness, is to combine the features of wave energy converters with other infrastructures, such as port infrastructures, which are becoming an emerging and prominent actor of the wave energy sector. In this context, OWC devices incorporated into caisson breakwaters for port infrastructures are one of the most promising technology for the exploitation of wave energy resource. In particular, the structural safety and global stability of OWCs under extreme wave events is a challenging task, at this stage of their early industrial development. For this reason, the stability analysis under extreme wave forces is a fundamental aspect, which has to be considered in the development of OWC breakwaters in order to prevent damage and destruction of such structures. Some initial studies (Pawitan et al., 2019; Viviano et al., 2019; Zhao et al., 2022) concern the mechanics of wave loads acting against a OWC incorporated into a breakwater, and on the estimation of wave pressures and of wave forces acting on these structures.

An innovative wave energy converter, belonging to the family o OWCs, is the U-OWC (or REWEC) plant, developed in the last decades. The U-OWC, compared with a conventional OWC, introduces substantial improvements useful in the perspective of wave energy exploitation. Moreover, the U-OWC device has been conceived for developing the construction of a cost-effective upright breakwater including an efficient wave energy collector. Based on full-scale application, the U-OWC breakwater is considered as one of the most effective harvesters for producing energy from sea waves, due to its capability to absorb a high percentage of the incoming wave energy. The U-OWC is able to absorb between 70 and 90 % in the sea states designed to reach the resonance condition, and between 50 and 70 % in other sea states (Arena et al., 2018).

The present paper focuses on the structural stability analysis of U-OWC breakwater with respect to wave forces due to non-breaking and breaking sea waves. The paper is organized as follows: the first section presents the properties of the U-OWC device, which has been largely validated both with small-scale field experiments and full-scale monitoring activity, and the set-up of a small-field experiment in the NOEL laboratory is presented; in the second and the third sections, the hydrodynamic response of the U-OWC device and the hydrodynamic forces realized in the active parts of the U-OWC (the U-duct and the inner pneumatic chamber) are evaluated; in the fourth section, the results of the small field experiment on wave pressures and wave loads acting on the modified U-OWC structure during extreme wave events are discussed; in the fifth section, the Quasi-Determinism (QD) nonlinear model at the U-OWC breakwater is introduced for the calculation of wave forces in the case of Qausi-Standing wave condition, and the analytical model is validated against field data; in the sixth section, the Goda's method is applied for the calculation of wave pressures on the U-OWC breakwater and the theoretical results are compared to the experimental ones; finally, the conclusions are presented in last section.

Table 1
Range of variability of significant wave height H_{S_i}, peak spectral period T_p, and the mean wave direction associated with the directional spectrum θ_m, and parameter ψ^* calculated in the records 1–771.

H_{S_i}	T_p	θ_m	ψ^*
(m)	(s)	(deg)	
0.12–1.12	1.6–9.8	−11–18	0.63–0.76

2. The small-scale field experiment on the U-OWC model incorporated into a caisson breakwater at the NOEL laboratory

2.1. Experimental set-up

The REWEC3 - *Resonant Wave Energy Converter, realization 3* (with independent absorbing chambers) is an innovative wave energy converter, which can be integrated into a caisson breakwater in reinforced concrete. The REWEC3 cross-section, compared to a classical Oscillating Water Column (OWC) device, consists of a pneumatic inner chamber connected to the open field via a U-duct. For this reason, the device is named also U-OWC. In this plant, a water mass is contained in the lower part of the chamber and in the U-duct; and an air pocket is located in the upper part of the pneumatic chamber. Then, the inner chamber is connected to the atmosphere via either an orifice or a tube, where a Power Take Off (PTO), such as a self-rectifying turbine coupled to an electrical generator, can be installed for the conversion of the absorbed energy into electricity.

The structural feature of the U-OWC device is quite similar to that of classical OWCs, although it introduces radically changes in the physics of the plant. Indeed, sea waves do not propagate inside the inner pneumatic chamber, but the wave pressure fluctuations at the opening of the vertical U-duct are able to induce water mass oscillations inside the duct/chamber; and, consequently, to generate an alternate air flow in the duct connecting the pneumatic chamber with the atmosphere. This fundamental property allows for achievement of the natural resonance without the use of any phase control devices required in the conventional OWC. More specifically, the natural resonance allows for the possibility to set the eigenperiod of the plant to be equal to the peak period of the most energetic sea states at the considered location, improving significantly the energetic performances of the U-OWC device (see Arena et al., 2018).

In the development of the U-OWC device, such as for all Wave Energy Converters (WECs), there are two equally important and complementary aspects: i) the optimization for the device with the aim to maximize the amount of electricity produced by the plant and ii) the structural reliability and overall stability for the survival of the device.

In this paper, the aspects related to the risk analysis under extreme wave forces acting on a caisson breakwater modified with U-OWC technology will be analysed and discussed.

In particular, a small-scale model (1:8 scale) of a U-OWC integrated into a caisson breakwater (Fig. 1*a*), installed off the beach of Reggio Calabria in the Eastern coast of the Strait of Messina (Southern Italy) at the Natural Ocean Engineering Laboratory (NOEL), is considered. The small-scale model of the caisson breakwater is in reinforce concrete and it is located at a water depth of 1.67 m. The U-OWC device is completely made of steel, and it is located in front of the concrete caisson (at the wave-beaten side) and structurally connected by rigid elements both in the bottom and in the lateral wall of its structure (Fig. 1*b*). The width of the U-duct is 0.5 m, while the pneumatic chamber is 1 m wide. The opening of the vertical U-duct is located at 0.57 m below the mean water level; and the top of the pneumatic chamber is long 3.04 m with respect to the U-opening, and it is equipped with a horizontal tube connecting the chamber to the atmosphere. In the transverse direction, the width of the active parts of the U-OWC (U-duct and pneumatic chamber) is 1.27 m.

A peculiarity of the laboratory is that a local wind from NNW often generates sea states consisting of pure wind waves that represent a small-scale model of Mediterranean or Ocean storms, in the Froude dynamic similarity (Boccotti, 2000). The experimental activities on the U-OWC caisson were executed from March to October 2015: the measurements were made continuously during the period considered.

During the experiment, the cross-section of the central caisson of the small-scale model was equipped with 28 pressure transducers (PTs). The scheme of the map of gauges at the U-OWC breakwater is given in Fig. 1*b*. Pressure transducer PT1 provides the wave pressure at the opening of the U-duct, useful for the evaluation both of the wave pressure acting on the external wall and of the excitation input of the plant. PTs from 2 to 10 are installed inside the inner pneumatic chamber, and they allow for achieving both of the particle velocity and acceleration of the mass water, and of the water level inside the chamber; PT11 provides a direct measure of the air pressure in the pneumatic chamber. Then, PTs from 12 to 14 are located along the external wall of the U-duct from the opening to the bottom, with centre distance of 0.45 m. Finally, PTs from 15 to 28 are installed along the external wall of the chamber in the wave-beaten side, with centre distance 0.15 m from 15 to 21, and 0.21 m from 22 to 28.

2.2. Characterization of wave conditions in the incident wave field

The free surface elevation and wave pressures of the incident waves are calculated through a set of instruments, located in the undisturbed wave field, far from the U-OWC structure (Fig. 1*a*). They are placed on two thin vertical piles, each equipped with a couple of an ultrasonic probe and a pressure transducer.

During the experiment, in the sample of recordings carried out from March to October 2015, a set of 771 records of pure wind waves were identified. The duration of each record was 5 min, with a sampling rate of 10 Hz, for the measurements both in undisturbed wave field and on the U-OWC structure. As showed by Peregrine (2003) and Boccotti et al. (2012), 10 Hz can be suitable for long analyses on wave forces in real field. Indeed, the small-scale field experiment on the U-OWC breakwater was carried out at NOEL laboratory involving measurements continuously for several months. During the experiments more than 10.000 sea states were recorded, but, for the purpose of the present work, only sea states of pure wind waves are examined. Moreover, in what follows, the wave pressures and wave forces on the U-OWC structure are analysed only considering average profiles associated with intense events, useful for the evaluation of overall stability of the modified breakwater (Boccotti et al., 2012). Instead, for different analyses involving the evolution of every single impact produced by a breaking wave on a seawall, and the impact formation on the structure, which can be correlated with the wave profile evolution, higher sampling rates are needed (10 kHz or more, as explained in Peregrine, 2003).

The range of variability of the main statistical quantities of sea states recorded during the field experiment, is summarized in Table 1. Specifically, it shows the significant wave height H_{S_i}, the peak spectral period T_p, and the mean wave direction associated with the directional spectrum, θ_m, of the free surface displacement in the undisturbed wave field. In addition, the narrow-bandedness parameter ψ^* of Boccotti (2000) for surface waves, defined as the absolute value of the ratio between the minimum and the maximum of the autocovariance function of the free surface displacement is calculated. The ψ^* value of wind-wave spectra is equal to 0.73 for the mean JONSWAP spectrum (Hasselmann et al., 1973) and to 0.65 for the Pierson and Moskowitz, (1964).

In the present study, only the records of pure wind-waves with single-peaked spectra similar to the JONSWAP-Mitsuyasu, are considered, since they give the more interesting features, which have to be considered in the structural design of a U-OWC breakwater. During the experimental campaign in the considered 771 recorded sea states, the ψ^* ranges from 0.63 to 0.76, typical of wind waves (Table 1). Moreover, the variation of the tide during the experimental campaign is within ±0.15 m. In particular, the sea storms considered have a significant wave

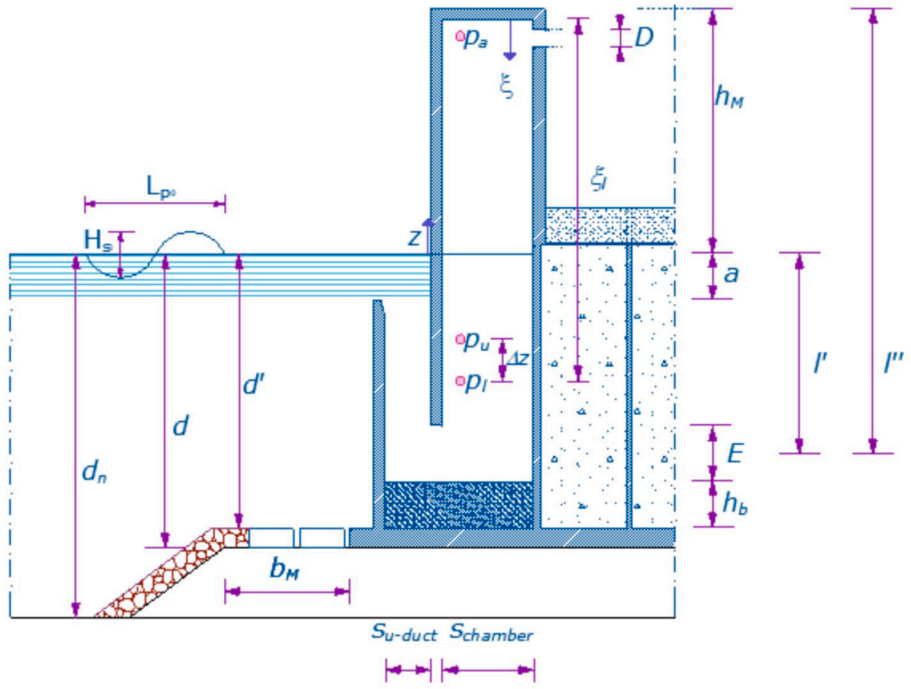

Fig. 2. Sketch diagram illustrating the geometry and the water depths in front and in the proximity of the U-OWC breakwater.

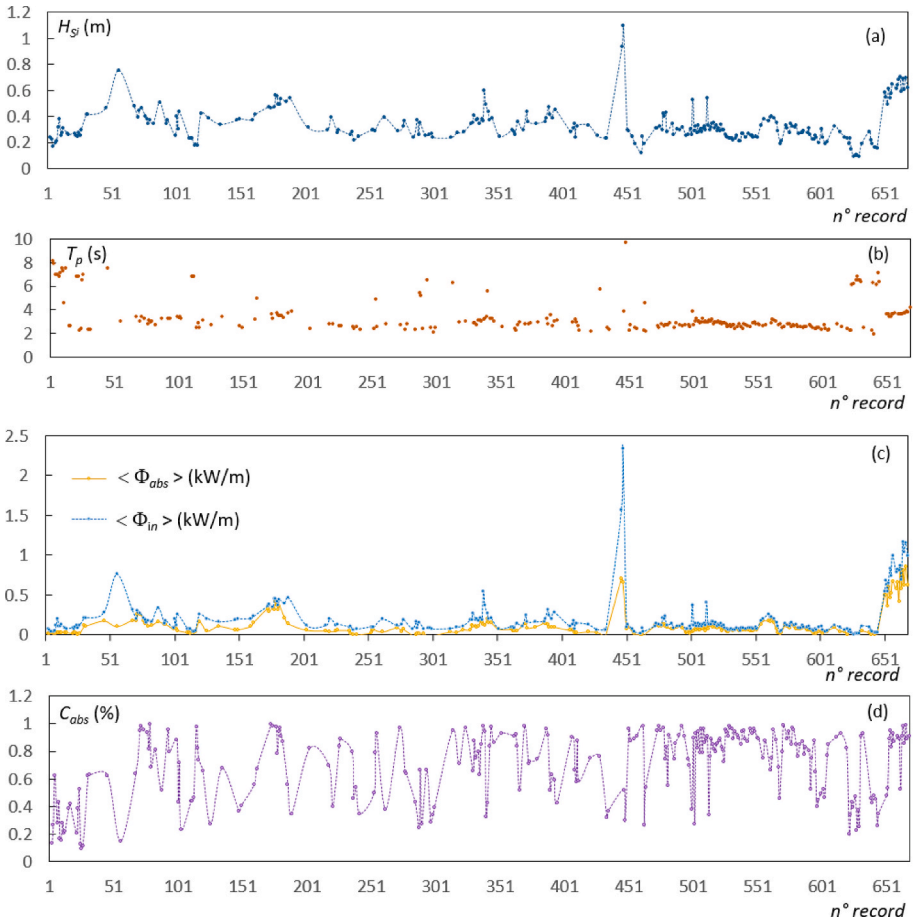

Fig. 3. Wave conditions at the U-OWC model during the small-scale field experiment at NOEL laboratory: (a) the significant wave height H_{S_i} and (b) the peak wave period T_p in undisturbed wave field. The average incident wave power Φ_{in} and average absorbed wave energy Φ_{abs} are given in panel (c) and the absorption coefficient is reported in panel (d).

height, H_{S_i}, ranging among 0.12–1.12 m and related peak period, T_p, typical of JONSWAP spectrum, varying in the interval 1.6–9.8 s (see Table 1).

3. The hydrodynamics of the U-OWC plant under different wave conditions

The U-OWC breakwater is a modified coastal defence structure able to absorb the wave energy of incoming waves. For this reason, first of all, an analysis of the hydrodynamics inside the U-OWC plant is pursued.

Specifically, the instantaneous acceleration a of the water column is calculated from the measured wave pressure inside the pneumatic chamber by the equation

$$a = \frac{p_l - p_u}{\rho \Delta z} - g \tag{1}$$

where p_l and p_u are the water pressures recorded simultaneously by two pressure transducers ("l", the lower and "u", the upper) located in the inner water column (in the present case, they are PTs 3–4 of Fig. 1*b*), Δz is the distance between the two gauges (see the sketch diagram Fig. 2), ρ is the water density and g is the gravity acceleration.

Then, following the procedure described by Boccotti et al. (2007), the instantaneous water column level ξ (positive downward and measured from the top of the air chamber, see Fig. 2), is calculated by the equation

$$\xi = \xi_l - \frac{p_l - p_a}{\rho(g + a)} \tag{2}$$

where ξ_l is the vertical distance between the lower instrument installed into the water column and the top of the U-OWC, and p_a is the air pressure inside the chamber measured by PT11.

Finally, starting from the time history of the U-OWC response, the absorbed wave energy is estimated by the capture width ratio (C_{abs}), given by

$$C_{abs} = \frac{< \Phi_{abs} >}{< \Phi_{inc} > b_x} \tag{3}$$

where $< \Phi_{abs} >$ is the average wave power absorbed by the U-OWC pneumatic chamber during a recorded sea state, $< \Phi_{inc} >$ is the wave energy resource per unit length available in front of the structure and b_x is the width of the chamber and of the U-duct in the transversal dimension.

Specifically, the average wave power $< \Phi_{abs} >$ is estimated by the approach of Boccotti et al. (2007),

$$< \Phi_{abs} > = - b_x s_{chamber} \frac{1}{T} \int_0^T \left[\Delta p_{U-OWC} + \frac{1}{2} \rho (\dot{\xi})^2 \left(\frac{s_{chamber}}{s_{u-duct}} \right)^2 \right] \dot{\xi} \, dt \tag{4}$$

where T is the record duration, Δp_{U-OWC} is the wave pressure measured at the top of the U-duct given by PT 1; $\dot{\xi}$ is the time derivative of the wave column displacement inside the active chamber; $s_{chamber}$ and s_{u-duct} are the widths of the pneumatic chamber and of the U-duct in the longitudinal dimension, respectively.

Then, for each record, the omnidirectional incoming wave power $< \Phi_{inc} >$ can be obtained by the following expression, valid in deep waters (Arena et al., 2015):

$$< \Phi_{inc} > = \frac{\rho g^2}{64\pi} \alpha_{f_1} H_{s_i}^2 T_p \tag{5}$$

where $< \Phi_{inc} >$ is the average wave power per unit length [kW/m], H_{S_i} is the significant wave height of incident waves [m], T_p is the peak period [s] (they are both determined in Section 1.2, and the values related to the small-scale field experiment are given in Table 1) and α_{f_1} is a spectral parameter equal to 0.91 for the mean JONSWAP spectrum and to 0.86 for the Pierson-Moskowitz spectrum.

In Fig. 3, the sea wave conditions in undisturbed wave field are illustrated. In particular, for each record the significant wave height of incident waves H_{S_i} is given in panel (a) and the peak wave period in panel (b) (see also Table 1). Then, in panel (c), the average wave power of incident waves, calculated via Eq. (5), and the average wave power absorbed per unit length by the U-OWC plant, estimated by Eq. (4) divided by b_x, are illustrated for each record. The response of the plant shows a high degree of efficiency during the field experiment executed at NOEL laboratory. Indeed, the C_{abs} factor is less than 0.5 for only the 20 % of the set of analysed records. Nevertheless, the plant reveals the capability to capture more than the 80 % of the incoming resource for a large number of sea states (45 % of the whole set) associated to moderate energetic seas.

4. The U-OWC hydrodynamic forces for the global stability of the modified structure

As explained in Section 1, in a U-OWC breakwater, the wave pressure fluctuation, Δp_{U-OWC}, due to sea waves acts at the U-opening producing the water mass oscillations in the U-duct and in the pneumatic chamber. Consequently, hydrodynamic forces are realized inside the U-duct and the inner chamber.

More specifically, the momentum flow through the plant is given by

$$F_{hydro_1} = \rho Q_p u - \rho Q_p \dot{\xi} \tag{6}$$

where Q_p is the water discharge of the plant, defined as

$$Q_p = - s_{u-duct} b_x u = - s_{chamber} b_x \dot{\xi} \tag{7}$$

with ρ the water density, u the water mass velocity in the U-duct (positive if outgoing to the U-duct), related to the water mass velocity in the pneumatic chamber, $\dot{\xi}$, through the continuity equation

$$u = \frac{s_{chamber}}{s_{u-dcut}} \dot{\xi} \tag{8}$$

Then, the dynamic forces associated with the acceleration of the water mass inside the plant are expressed by

$$F_{hydro_2} = \rho \, l' A' \dot{u} - \rho \, (l'' - \xi) A'' \ddot{\xi} \tag{9}$$

where l' and l'' are the length of the vertical duct and of the inner chamber, referred to $E/2$, respectively (see Fig. 2); and $\dot{u}$ and $\ddot{\xi}$ are the water mass acceleration in the U-duct and in the pneumatic chamber, respectively.

Finally,

$$A' = s_{u-duct} b_x \tag{10}$$

is the area of the U-duct and

$$A'' = s_{chamber} b_x \tag{11}$$

is the area of the inner chamber. It is noted that both hydrodynamics forces F_{hydro_1} and F_{hydro_2} are null, because their contributions at the U-opening (the first terms of both Eqs. (6) and (9)) and inside the chamber (the second terms of both Eqs. (6) and (9)) balance each other out.

Moreover, associated to the variation of the instantaneous water column level, an additional contribution to the weight force is realized inside the pneumatic chamber, which is

$$F_{hydro_3} = \rho g (\xi_0 - \xi) A'' \tag{12}$$

where ξ_0 is the water level in still conditions. This force is balanced by the equal and opposite reaction produced by the roof of the absorption chamber.

Finally, two surface forces are realized in the active parts of the U-OWC breakwater. The first one is at the water interface of the U-duct and

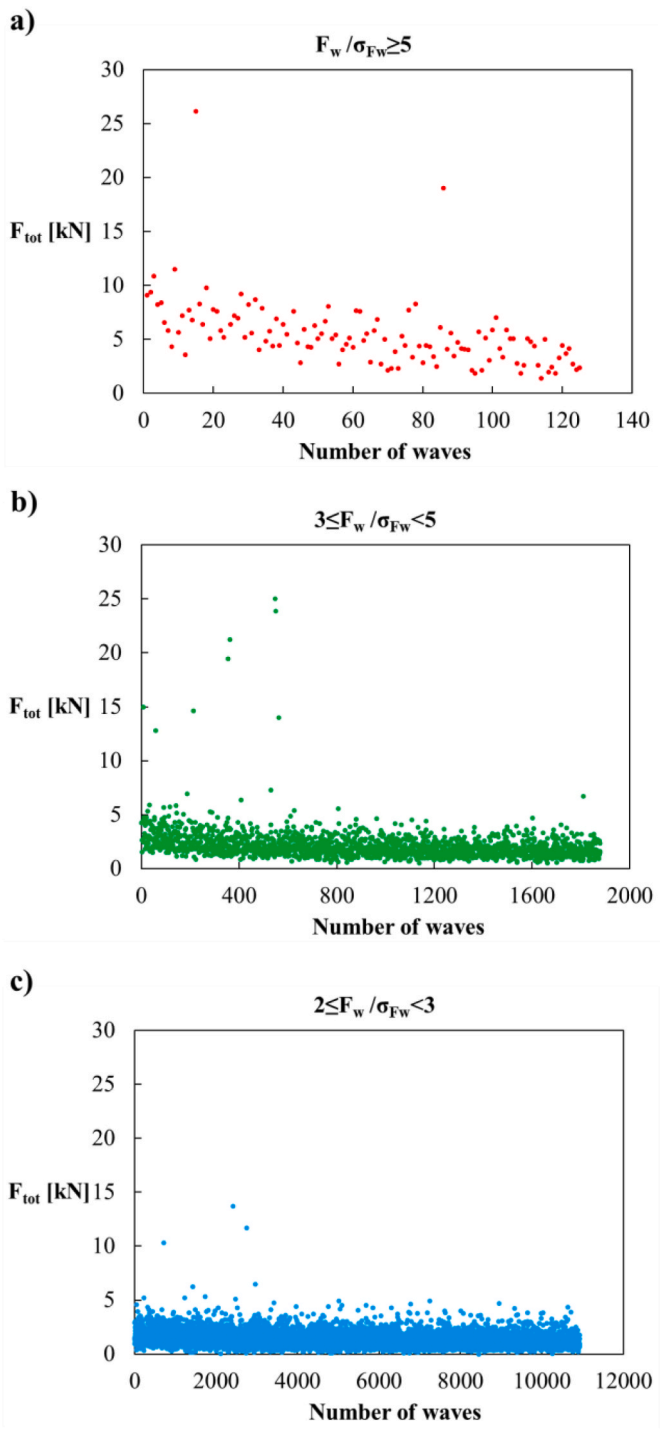

Fig. 4. The total hydrodynamic force $F_{tot} = F_{hydro_4} + F_{hydro_5}$, calculated via Eq. (15) for all the positive peaks of the wave force $F_w(t)$ realized at the U-OWC modified breakwater. The measured total force is due to the hydrodynamics inside active parts of the U-OWC, and it is calculated for three ranges of positive peak forces recorded on the external walls: (a) $F_w/\sigma_{F_w} \geq 5$; (b) $3 < F_w/\sigma_{F_w} < 5$; (c) $2 < F_w/\sigma_{F_w} < 3$. In the case (a) H_{S_i} ranges in 0.2–0.53 m; in the case (b) H_{S_i} varies among 0.4–0.79 m; in the case (c) H_{S_i} is among 0.64–1.2 m.

it is given by

$$F_{hydro_4} = \Delta p_{U-OWC} A' \tag{13}$$

where Δp_{U-OWC} is the wave pressure fluctuation at the U-opening, measured by PT1, and A' is calculated by Eq. (10). The additional surface

Fig. 5. The small-scale model of U-OWC breakwater at NOEL laboratory during a sea storm with the realization of wave loads on the structure.

force occurs at the air/water interface inside the inner pneumatic chamber, and it is defined as

$$F_{hydro_5} = (p_a - p_{atm})A'' \tag{14}$$

where p_a is the air pressure inside the pneumatic chamber measured by PT11, and p_{atm} is the atmospheric pressure; A'' is calculated by Eq. (11).

In conclusion, only F_{hydro_4} and F_{hydro_5} can affect the overall stability of the structure. In details, the resultant of these two forces, defined as

$$F_{tot} = F_{hydro_4} + F_{hydro_5} \tag{15}$$

is the only additional hydrodynamic force, which contributes to the global stability of the modified U-OWC structure compared to those of a traditional breakwater. If positive, it is directed downwards increasing the overall stability of the U-OWC breakwater, otherwise upwards and, thus, producing instability of the modified structure.

In Fig. 4, the hydrodynamic force F_{tot} inside the plant is evaluated via Eq. (15), when a positive peak force, given by sea waves acting on the modified structure, occurs at the U-opening. This means that a wave crest of surface elevation is realized on the front wall of the structure, because a positive force corresponds to a crest of surface waves. In Fig. 4, the F_w is the wave force per unit of length, acting on the external walls of the U-OWC breakwater of the NOEL field experiment and σ_{F_w} is its own standard deviation; in detail, F_w is calculated at the mid-section of the U-OWC device by integrating the wave pressure measured by the set of pressure transducers installed along external walls of the breakwater, as illustrated in Fig. 1*b*. For further details, we refer to the next Section. In particular, for the purpose of investigation of hydrodynamic forces inside the U-OWC device, from the time series of the recorded wave force $F_w(t)$ acting on the modified structure on external walls of the active

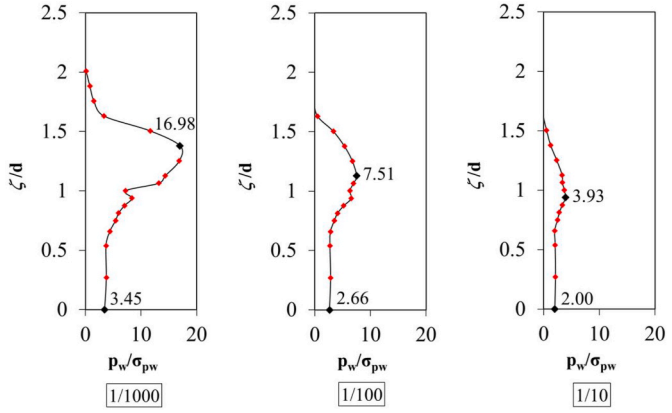

Fig. 6. Average wave pressure distribution corresponding to the greatest $N/1000$, $N/100$ and $N/10$ positive force peaks $\widetilde{F}_w(t)$ based on the whole dataset of 771 records.

Table 2
Dimensionless coordinates of the pressure transducers along the external wall of the U-duct (PTs from 12 to 14) and of the pneumatic chamber (PTs 1 and from 15 to 28) of the U-OWC caisson, related to the depth d equal to 1.67 m.

Pressure Transducer (PT)	ζ/d
12	0
13	0.269
14	0.539
1	0.659
15	0.751
16	0.813
17	0.876
18	0.939
19	1.002
20	1.065
21	1.128
22	1.254
23	1.379
24	1.505
25	1.631
26	1.757
27	1.882
28	2.008

parts, all the positive peaks are selected and the corresponding hydrodynamic forces, F_{hydro_4} and F_{hydro_5}, realized inside the plant, are calculated. Their resultant F_{tot} is given in Fig. 4, for some ranges of positive peaks recorded in the front walls of the U-OWC breakwaters. It is shown as F_{tot} is always positive, with greater intensity when the impacts are more violent. In practice, when a wave crest of surface wave occurs at the U-OWC breakwater, the hydrodynamics inside the plant generates a global additional force, which contributes to increase the overall stability of the modified U-OWC caisson breakwater under the action of a wave crest.

Consequently, the proper estimation of the maximum total horizontal wave force on the front walls and of the uplift force (vertical force due to sea waves) on the base of the caisson are fundamental for evaluating the overall stability of the breakwater modified with U-OWC technology. Indeed, these wave forces are the only ones that can produce the instability of the U-OWC structure. These aspects will be investigated in the next sections.

5. Wave pressure and horizontal wave loads on the model of U-OWC breakwater

5.1. Post-processing data of the small-scale experiment on the U-OWC breakwater deployed at NOEL laboratory: wave pressure and horizontal wave loads

In this section the post-processing data of the small-scale field experiment on the U-OWC model installed at the NOEL laboratory is pursued in order to investigate the wave pressures and horizontal wave forces acting against the modified U-OWC breakwater.

During the small scale field experiment, a large number of severe wave loads on the modified structure have been observed. In this regards, a sequence of intense wave loads on the model of U-OWC breakwater is reported in the pictures of Fig. 5.

Starting from the observations, the wave loads acting on the U-OWC breakwater installed at NOEL are investigated by considering the set of pressure transducers (PTs – Fig. 1*b*), that is to say PT1 and PT from 12 to 28, installed along the external walls both of the U-duct (PT12-14) and of the pneumatic chamber (PT1,15–28).

In details, for each sea state, the recorded time series of wave pressure $p_{w_{PT_i}}(t)$ (PTi = 1, 12–28) along external walls are considered. Consequently, the wave force $F_w(t)$, per unit of length, at the mid-section of the U-OWC breakwater is calculated by integrating the pressure distribution recorded by the array of eighteen pressure transducers (PTi = 1, 12–28), deployed as shown in Fig. 1*b* (PT12 being the pressure transducer at the bottom of the modified structure and PT28 the pressure transducer at the top of the U-OWC breakwater).

Then, for each sea state, both the dimensionless wave pressures and the dimensionless wave forces are computed. In detail, the dimensionless wave pressures at every depth are given by dividing the recorded $p_{w_{PT_i}}(t)$ (PTi = 1, 12–28) by its own standard deviation σ_{p_w}. Then, the dimensionless force $\widetilde{F}_w(t)$, is obtained by dividing the measured force $F_w(t)$ by its own standard deviation σ_{F_w}, and it is calculated for each recorded sea state as:

$$\widetilde{F}_w(t) = \frac{F_w(t)}{\sigma_{F_w}} \tag{16}$$

The positive peaks of the $\widetilde{F}_w(t)$ random process are determined for all the sequence of every 5-min records. In this paper, we define the '*positive peak force*' as the crest of the recorded dimensionless wave forces $\widetilde{F}_w(t)$ in time domain, and the '*number of waves*' is the number of zero up-crossing waves of the normalized random wave-force-process, $\widetilde{F}_w(t)$ (Eq. (16)). Accordingly, to each positive peak force corresponds a measured wave pressure distribution acting on the external walls of the structure.

The number N of zero up-crossing waves of the normalized random wave force process, $\widetilde{F}_w(t)$, in the sequence of the records during the whole dataset of the experiment, are equal to 84,849. Then, the greatest $N/1000$, $N/100$ and $N/10$ positive peaks of the $\widetilde{F}_w(t)$ process are identified, and the related average dimensionless wave pressure distributions are calculated. They are showed in Fig. 6, where dots denote the measured wave pressures on the front walls of the U-duct and of the pneumatic chamber at the U-OWC model and ζ_i/d (i = 1,12–28) are the dimensionless coordinates of the pressure transducers along the external walls, related to the water depth d equal to 1.67 m (see Table 2).

It is shown that passing from the average wave pressure distribution of the $N/10$ maxima peak forces to that of the $N/100$ and $N/1000$ maxima, the maximum value recorded increases of about two and four times, respectively. Moreover, two other distinctive behaviours are recognized: i) for the $N/1$ 000 average wave pressure distribution, the wave pressure at bottom is about 1.7 times that recorded for the $N/10$ distribution; ii) the maximum dimensionless wave pressure is realized approximately at the mean water level in the $N/10$ distribution (ζ/d = 0.94) and it, increasing strongly in magnitude, occurs significantly

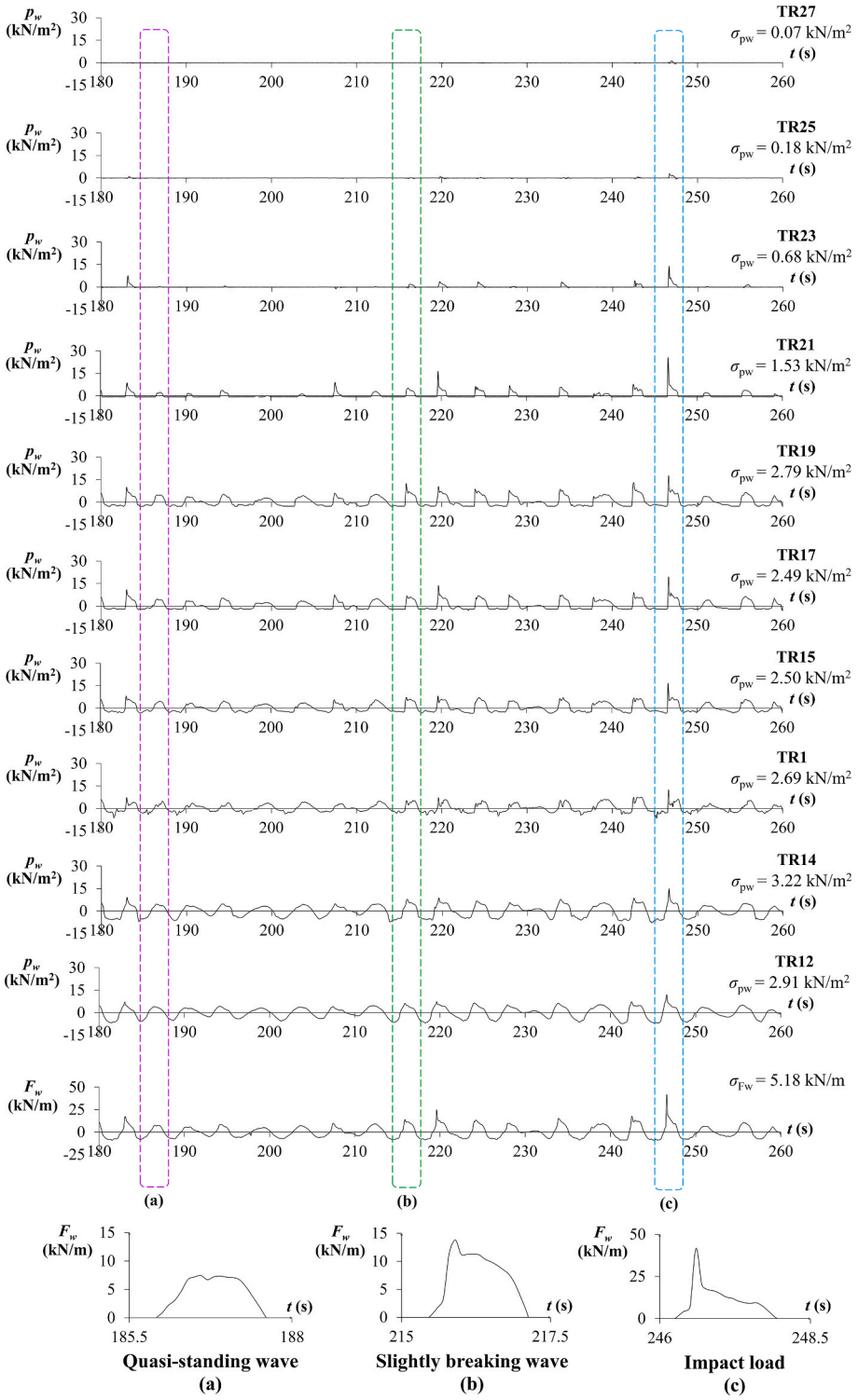

Fig. 7. Record 669, with $H_s = 0.618$ m and $T_p = 4.17$ s, and absorption coefficient, C_{abs}, during the measurement equal to 0.91. The complete time series of both the wave pressures and of the wave force on the external walls of active parts in the U-OWC model is given, identifying the occurrence of three wave load conditions: (a) Quasi-Standing wave: (b) Slightly Breaking wave; (c) Impact Load.

above the still water level in the $N/1\ 000$ distribution ($\zeta/\ d\ =\ 1.38$). This means that the most severe sea waves, recorded during the experiment, show the predominance of impulsive wave forces, due to wave breaking against the U-OWC structure. Indeed, it is well known in the literature (Oumeraci et al., 1993; Peregrine, 2003) that when the impulsive loads due to breaking sea waves are becoming prevalent with respect to those associated with quasi-standing waves, the maximum wave pressure increases strongly in intensity and it moves from the mean water level (quasi-standing waves in reflection and quasi-statics loads) to the middle transverse section of the classical seawall (breaking sea waves and impulsive loads). These behaviours are recognized in Fig. 6. In particular, by considering the most severe wave impacts, which correspond to the $N/1000$ wave pressure distribution, the maximum wave pressure is 16.98 σ_{p_w}, about 5.4 times greater than

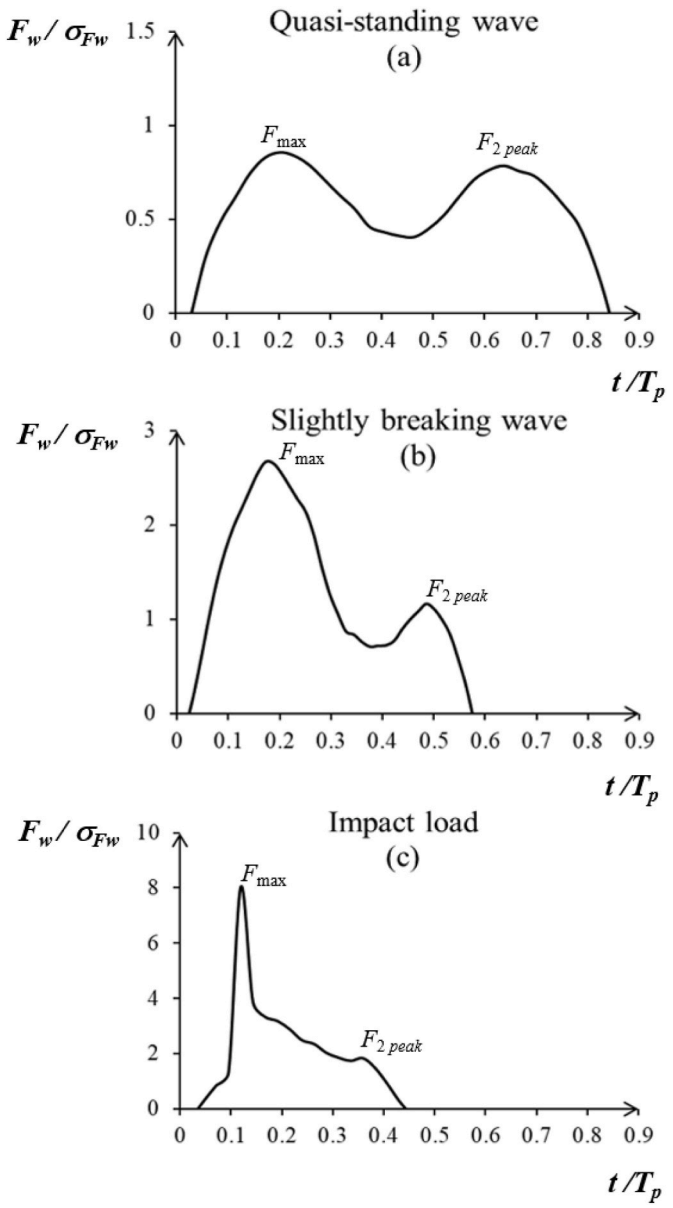

Fig. 8. Time series recorded at Noel characterized by the three wave loads $\widetilde{F}_w$ conditions realizing at the U-OWC breakwater (the time instant t is related to the peak period T_p): (**a**) Quasi-Standing wave with two positive peaks of about equal intensity; (**b**) Slightly Breaking wave with $F_{max}/F_{2peak} = 2.29$; (**c**) Impact Load with $F_{max}/F_{2peak} = 4.38$. Severe realizations during the field experiment of both SBW and IL loads are showed.

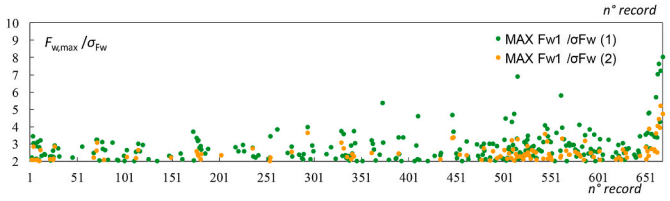

Fig. 9. Wave loading conditions at the U-OWC model during the small-scale field experiment at NOEL laboratory: the absolute maximum and the subsequent positive peak of the wave forces on the U-OWC model are given for each record.

Table 3
Number of waves of $\widetilde{F}_w(t)$ for the three conditions of wave loads.

Quasi-Standing Waves	Slightly Breaking Waves	Impact Loads
9010	4230	911

the maximum pressure recorded considering the $N/10$ wave pressure distribution, and it occurs above the mean water level, in the middle section of the external U-OWC pneumatic chamber.

Thus, an in-depth analysis of the recorded pressure time series is performed. For instance, in Fig. 7 the time series of both wave pressures along the external walls of the U-OWC structure and of the horizontal wave force are illustrated. The time series data are relative to record 669, characterized by a high degree of energy efficiency - the absorption coefficient, C_{abs}, being equal to 0.91 - and by the realization of intense wave loads both 'pulsating' and 'impulsive'.

In this regards, in the time series of the wave force process $\widetilde{F}_w$, we recognize some distinctive behaviors, which identify three classes of wave loads. In detail, if more than one positive peak force can occur in the same wave (see Fig. 7), the highest positive peak is denoted by F_{max}, while the second peak more intense is indicated by F_{2peak}. When F_{max} is comparable to F_{2peak}, a "Quasi-Standing Wave (QSW)" is realized (panel (*a*) of Fig. 7); if $1 < F_{max}/F_{2peak} < 2.5$, a "Slightly Breaking Wave (SBW)" occurs (panel (*b*) of Fig. 7); for $F_{max}/F_{2peak} > 2.5$, an "Impact Load (IL)" is considered (panel (*c*) of Fig. 7). By comparing panels a), and c) of Fig. 7, we notice that the impact loads can be approximately 5–6 times greater than the quasi-static ones. Moreover, the peak duration decreases significantly, when the peak intensity increases greatly.

This aspect is more remarkable in Fig. 8, where it is shown that when the double peaks of the wave force are of about equal intensity, the duration of the each positive impact is approximately 0.3 and 0.5 times the peak period T_p (see panel a); while, when the record shows an intense first maxima, F_{max} , with respect to second one, F_{2peak}, the duration of the positive impact is strongly reduced, being almost 1/100 T_p (panel c). Accordingly with Cuomo et al. (2010), we can consider also for the U-OWC breakwater that condition (*a*) of Fig. 8 associated to "quasi-standing" waves, is referred to sea waves not affected by the breaking phenomenon, which provide 'pulsating' or 'quasi-static' wave loads. When the wave load on the U-OWC breakwater is characterized by an intense positive peak with short duration (as "Slightly Breaking Waves" of panel (*b*) and "Impact Loads" of panel (*c*) of Fig. 8) an 'impulsive' condition, due to breaking waves, occurs at the modified structure.

Finally, the intensity of the wave loads is correlated to the operational conditions of the U-OWC. In Fig. 3, the absorption coefficients for all the considered 771 records are illustrated. Then, in Fig. 9 for the same sequence of records, the maximum positive peak and the subsequent second peak of the recorded wave force are showed. In all the records, the previous-called "Impact Loads" can be observed, showing that even when the U-OWC device is able to absorb the greatest percentage of the incoming wave energy (more than 80 %), extreme wave loads can occur on the external walls with positive peaks greater than 7 σ_{F_w}, σ_{F_w} being the standard deviation of the recorded wave force.

5.2. Identification of different wave load conditions and wave pressure distributions acting on the U-OWC model

Based on observations showed in Figs. 7–9, the phenomenon of wave impacts, due both 'quasi-standing' and 'impulsive' wave forces, is investigated during the small-scale field model of U-OWC breakwater deployed at the NOEL laboratory.

In Table 3, the number of waves of the wave-force-process $\widetilde{F}_w(t)$ for the three cases of impact wave loads, identified in the previous section, are indicated. Then, Fig. 10 shows the average dimensionless wave pressure distributions given by the $N/10$, $N/100$ and $N/1000$ highest

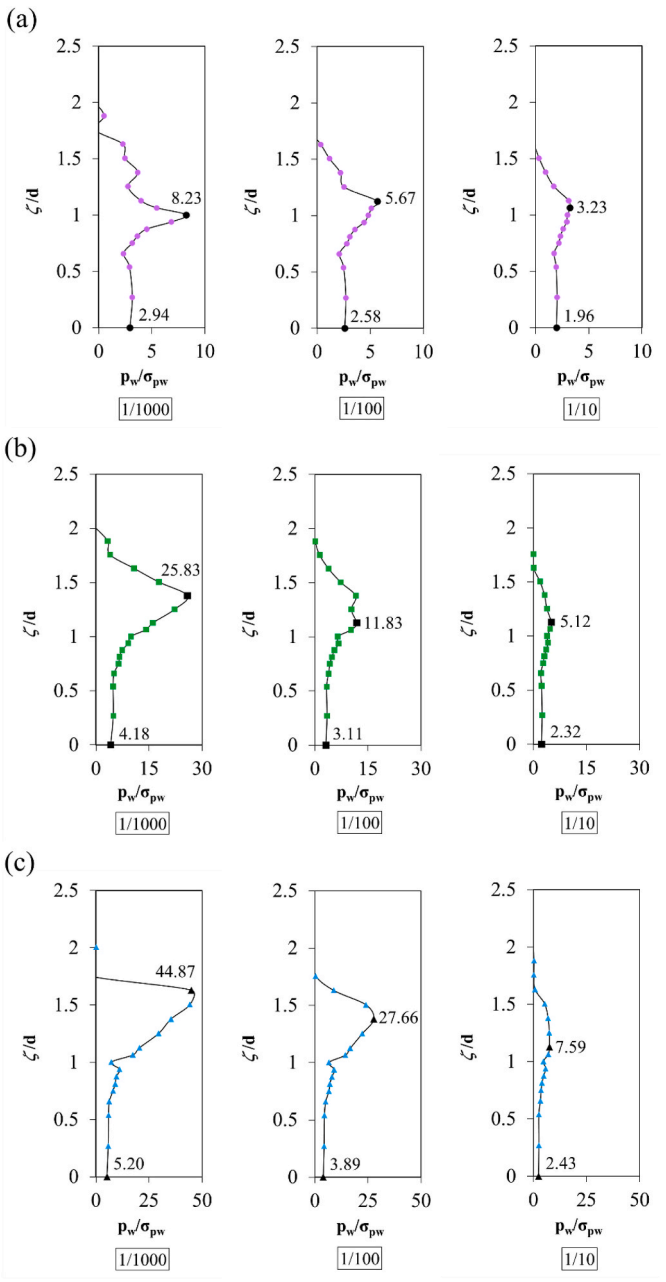

Fig. 10. Average wave pressure distribution corresponding to the greatest $N/1000$, $N/100$ and $N/10$ positive force peaks $\widetilde{F}(t)$ of: (a) the 9010 "Quasi-Standing waves"; (b) of the 4230 "Slightly Breaking waves"; (c) and of the 911 "Impact Loads".

positive peak force of the Quasi-Standing Waves, Slightly Breaking Waves and Impact Loads, respectively.

Considering the $N/10$ pressure distributions, the three wave loads configurations differ about 60 % in terms of maximum values, as it is appreciable comparing rights panels (*a*), (*b*) and (*c*) of Fig. 10. These differences become strongly remarkable when the $N/1000$ pressure distributions of highest positive peaks of wave forces are examined. That happens because the influence of the impulsive wave loads, characterized by peaks of a short duration but with a high intensity, becomes predominant. In fact, as shown in Fig. 10 (panel *a*), the maximum wave pressure measured, corresponding the $N/1000$ maximum forces, for the condition of "Quasi-Standing Waves (QSW)" is 8.23 σ_{p_w}. This value is almost triple when "Slightly Breaking Waves (SBW)" are realized (see Fig. 10 panel *b*), becoming even 44.87 σ_{p_w} for the case of "Impact Loads (IL)" (see Fig. 10 panel *c*), when the impulsive loads due to wave breaking are prevalent. It is noticed that, during the field campaign, the highest impact load measured had a peak equal to 8.67 σ_{p_w} (See Fig. 9).

Another important feature is also clearly highlighted passing from "Quasi-Standing Waves" to "Impact Loads": the greatest wave pressure occurs at a coordinate ζ/d higher than that of the mean water level ($\zeta/d = 1$). For the $N/1000$ average maximum pressure distributions, this coordinate is equal to 1.4 (which coincides with a height of 0.63 m above the m.w.l.) for the "Slightly Breaking Waves" and 1.63 for the "Impact Loads" (equal to a height of 1.00 m above the m.w.l.). This confirms that when the impulsive loads due to breaking sea waves are becoming dominant, the most critical point for risk of structural damage is the middle transverse section of the external U-OWC pneumatic chamber.

Finally, the field experiment has shown that the average maximum $N/1000$ horizontal wave force acting on the U-OWC breakwater can increase up to 5 times for sea states with prevalent breaking waves (Fig. 10 – panel *c*) compared to sea states with stable incoming waves ("Quasi-Standing Waves" in Fig. 10 – panel *a*); strongly increasing the wave forces, which can affect the global stability of the active modified coastal structure.

5.3. Wave loads on the U-OWC model based on a parametric analysis

During the experiment in real field, it is observed that for this kind of caisson breakwater in reinforce concrete modified with U-OWC technology for the wave energy absorption, a number of physical and structural conditions influence the mechanics of impact on the structure and, thus, the occurrence of the related wave loads acting on it.

The most significant are the structure geometry, the seabed topography in front and in the proximity and in front of the breakwater, the steepness and the spectrum of incoming waves, the non-linearities.

For this reason, in the present study, a set of parameters are selected to investigate their influence in the realization of the wave loads against the U-OWC modified breakwater.

In particular, for considering the influence of the seabed topography in front of the U-OWC breakwater, we consider the water depths of the caisson installation and of the berm (see Fig. 2) related to the significant wave height of incoming waves; that is to say

$$\frac{H_{S_i}}{d_n} \tag{17}$$

$$\frac{H_{S_i}}{d} \tag{18}$$

Moreover, the presence of the U-duct in the front side of the structure reduces significantly the depth, when the sea waves approach to the modified breakwater, before their impact. For this reason, the parameter of the wave height related to the depth of the device opening, a, is considered

$$\frac{H_{S_i}}{a} \tag{19}$$

Finally, when the incoming waves approach to the U-OWC breakwater, the horizontal length both of the berm before the structure and of the U-duct influences the wave impact on the innovative breakwater. Thus, the following two parameters are considered

$$\frac{b_M}{L_{p0}} \tag{20}$$

$$\frac{s_{u-duct}}{L_{p0}} \tag{21}$$

In Eqs. 17–21 H_{S_i} is the significant wave height of incident waves, $L_{p0}(=gT_p^2/2\pi)$ is the wavelength on deep water related to the peak period T_p, d_n (=2.67m) is the depth at the berm foundation, d (=1.67m)

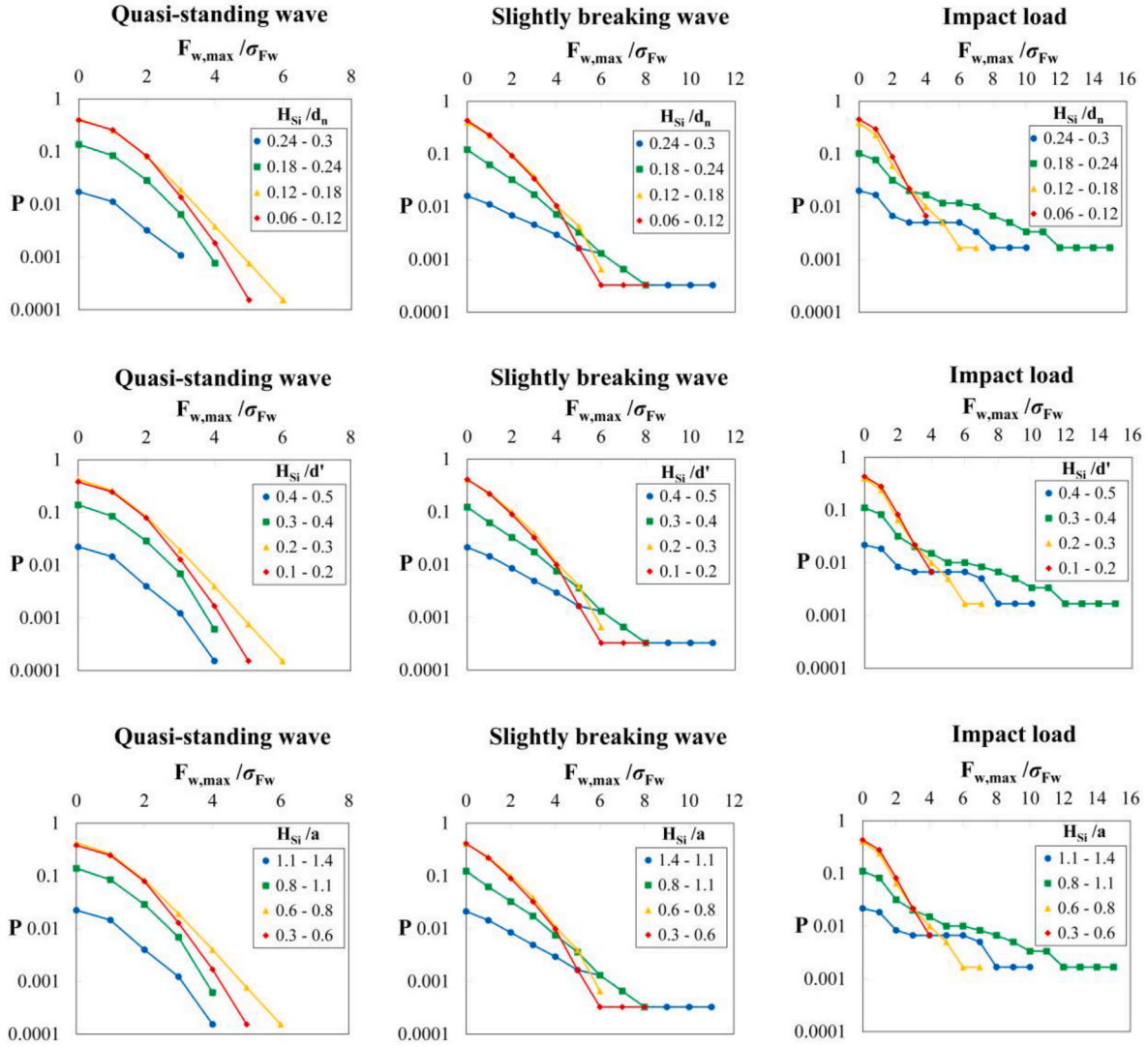

Fig. 11. Probability of exceedance of the maximum positive peak forces $P(F_{\max\_class_i} > \lambda)$ with $class_1$ = Quasi Standing waves, $class_2$ = Slightly Breaking waves, $class_3$ = Impact Loads, determined for the following key parameters: H_{Si}/d_n , H_{Si}/d', H_{Si}/a

is the depth where the U-OWC breakwater is deployed, b_M (=3.3m) is the length of the berm, a (=0.57m) is the depth of the outer opening of the U-duct, s_{u-duct} (=0.5m) is the width of the U-duct in the transversal dimension.

Moreover, the Ursell number U_r is considered for investigating the influence associated to non-linearities of incoming waves approaching to the U-OWC model. The definition of U_r is provided as,

$$U_r = \frac{H_{S_i}}{k_1 d'^3} \tag{22}$$

where $k_1 (= (2\pi)^2 / (gT_{m_{01}}^2))$ is the wave number of the mean wave period $T_{m_{01}}$ related to the zeroth-order and first-order moments of the frequency spectrum. Some authors evaluate U_r using peak wave period (T_p). In particular, following Arena and Pavone (2006) for the JONSWAP spectrum, the Ursell number can be calculated as follows

$$U_r = \frac{\alpha_{PH}^{0.5}}{2\pi^3} \frac{m_{w_0}^{4.5}}{m_{w_1}^4} \frac{1}{\left(d/L_{p0}\right)^3} \tag{23}$$

where α_{PH} is the Phillip's parameter ranging in the interval $(0.008 - 0.012)$, $L_{p0} (= gT_p^2/2\pi)$ is the wave length on deep water related to the peak period, m_{w_j} denotes the jth order dimensionless moment of the frequency spectrum, and the ratio $m_{w_0}^{4.5}/m_{w_1}^4$ is equal to 0.16 for the Pierson–Moskowitz spectrum ($\gamma = 1$) and to 0.27 for the mean JONSWAP spectrum ($\gamma = 3.3$).

The probability of exceedance of the maximum positive peak forces, for each class of wave loads considered in the study, is calculated:

$$P\left(F_{\max\_class_i} > \lambda\right) = \frac{N_{F_{\max\_class_i}}}{N_{tot\_class_i}} \quad i = 1, 2, 3 \tag{24}$$

where $class_1$ = Quasi Standing waves, $class_2$ = Slightly Breaking waves, $class_3$ = Impact Loads, and $N_{F_{\max\_class_i}}$ are the number of maximum positive peaks above a certain threshold λ and $N_{tot\_class_i}$ the total number of maximum positive peaks, for each wave load conditions (the values are reported in Table 3), respectively.

This probability distribution of a maximum peak force is calculated by Eq. (24) starting from dataset of the field experiment on the U-OWC model breakwater at NOEL laboratory. Thus, a parametric study is pursued considering the key parameters, defined from Eq. (17)–(22), involved in the computation and useful for different practical applications. The results of calculations are shown in Figs. 11 and 12, where the exceedance probability (24) is calculated given the various parameters introduced. The results highlight the high influence of each parameter in the occurrence of the maxima peak forces on the U-OWC breakwater. In

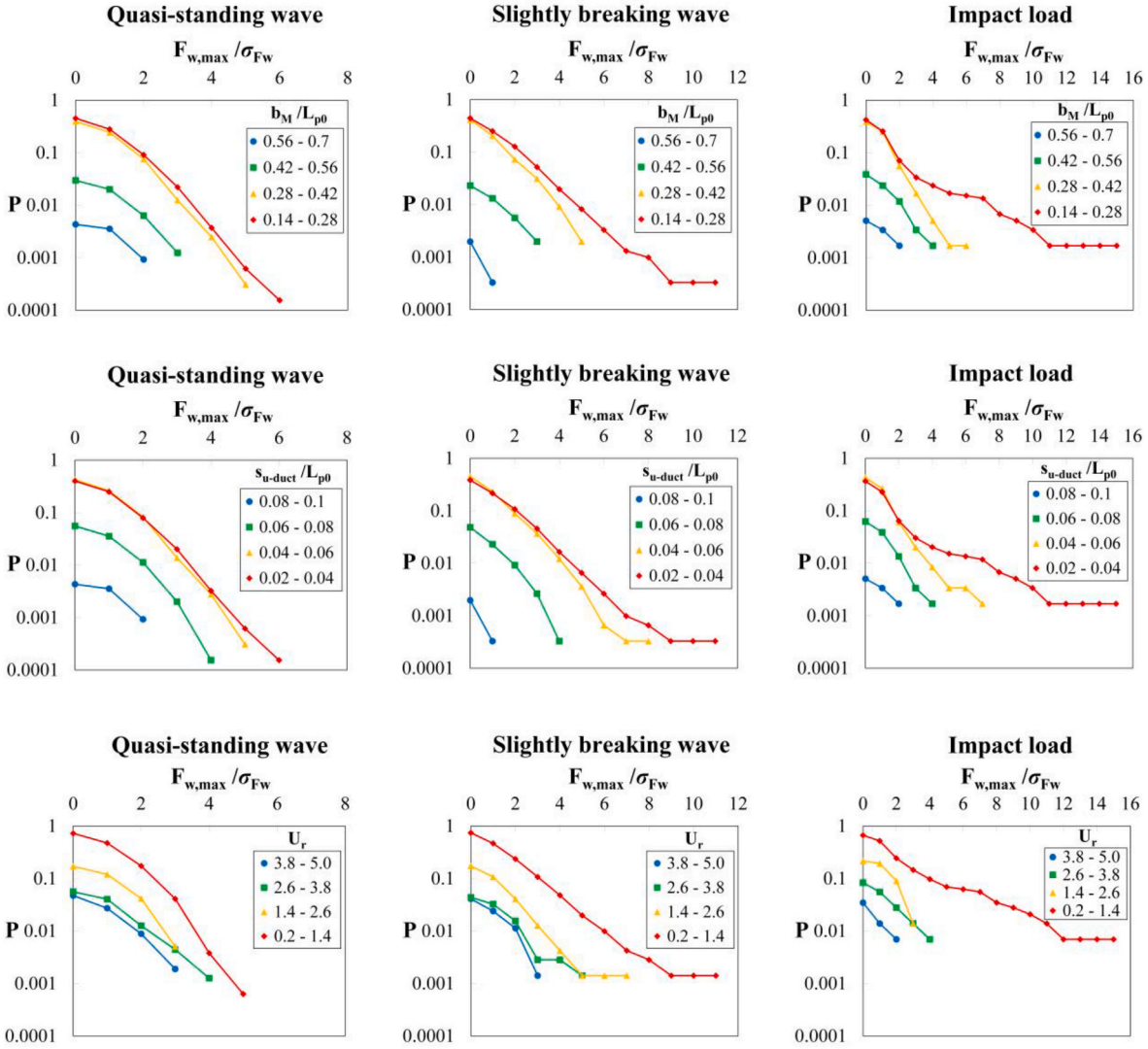

Fig. 12. Probability of exceedance of the maximum positive peak forces $P(F_{\max\_class_i} > \lambda)$ with $class_1$ = Quasi Standing waves, $class_2$ = Slightly Breaking waves, $class_3$ = Impact Loads, determined for the following key parameters: b_M/L_{p0} , s_{u-duct}/L_{p0}, U_r

Table 4
The significant wave height H_{si}, the related peak period T_p, and the recorded β coefficient with dominant wave direction orthogonal to the U-OWC breakwater, for the five most intense records of Quasi-Standing wave pressure distributions illustrated in Figs. 13 and 14.

Record	H_{si} (m)	T_p (s)	β recorded
136 corresponding to the first positive peak of the QSW wave force	0.393	3.12	0.556
264 corresponding to the second positive peak of the QSW wave force	0.311	2.83	0.671
258 corresponding to the third positive peak of the QSW wave force	0.357	2.68	0.540
165 corresponding to the fourth positive peak of the QSW wave force	0.351	3.00	0.620
60 corresponding to the fifth positive peak of the QSW wave force	0.548	3.12	0.395

Fig. 11, the influence of the significant wave height of incoming waves H_{S_i} with respect to both the water depths d_n , d, (see Fig. 2) and to the depth of the U-opening a is examined. Considering Quasi-Standing waves, the maxima positive peak forces are realized for deeper water depths d_n given a fixed significant wave height H_{S_i}. Instead, for "Slightly Breaking waves"; and "Impact Loads", the extreme loads are recorded for the most intense sea states, with greater H_{S_i} , and for decreasing water depth d_n. Indeed, for fixed value of probability of 1/1000, in the case of QSWs, the maxima peaks of the wave force $F_{w_{\max}}$ are equal in magnitude to 3 σ_{F_w} and they occur when the ratio H_{s_i}/d_n ranges in [0.12 – 0.18]. Moreover, for the SBW and IL conditions, the maxima peak forces are recorded when the range of H_{s_i}/d_n is [0.18 – 0.24], and they are, respectively, about 8–10 σ_{F_w} and 12-16 σ_{F_w} for the threshold 1/1000 of the probability of occurrence.

The same behaviors are given by considering the influence of H_{S_i} with respect to the water depths d, and a (see the two lower left panels of Fig. 11). In particular, in the modified breakwater, for given significant wave height of incoming waves H_{S_i}, when the depth a of the U-opening is reduced, violent wave loads are recorded with extreme positive peaks of the wave forces up to 16 σ_{F_w}, σ_{F_w} being the standard deviation of the recorded wave force. These extreme loading conditions are relative to impulsive wave loads (IL – see right and lowest panel of Fig. 11), which are due to the breaking waves acting against modified structure and caused by the reduction of the depth of the U-opening. These extreme loads can also occur when the significant wave height increases at a fixed depth of the U-opening, a.

Then, the influence both of the length of the berm, b_M, and of the width of the U-duct, s_{u-duct} , is illustrated in Fig. 12. For fixed values of

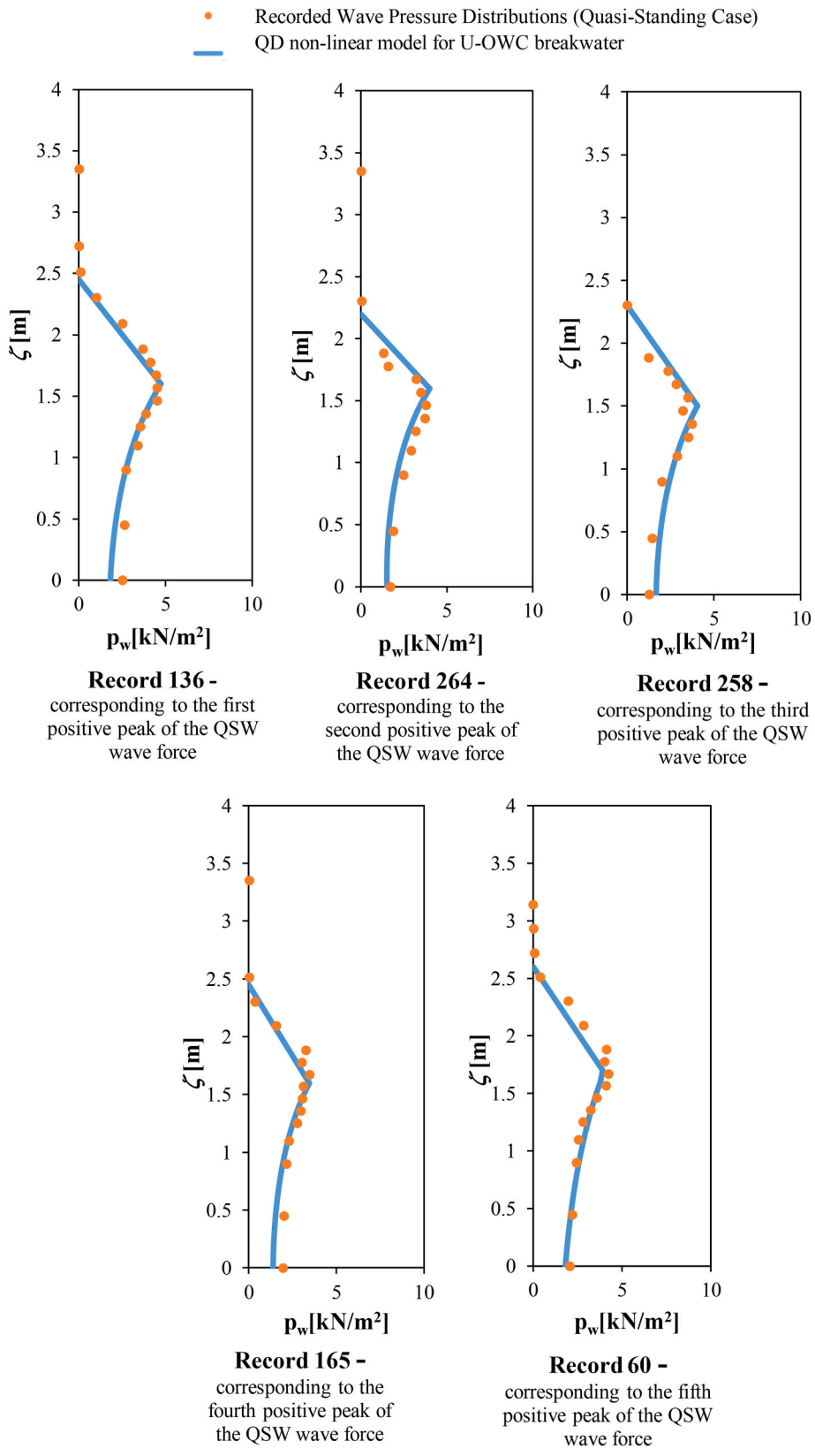

Fig. 13. Pressure distributions relative to the first 5 greatest positive force peaks $\widetilde{F}(t)$ for "Quasi Standing waves" versus QD nonlinear model at the U-OWC breakwater.

Table 5
The recorded wave force $F_{w,\max\_recorded}$ acting on the U-OWC model, the wave force $F_{w,\text{QD nolinear\_U-OWC}}$ calculated via the QD nonlinear model at the U-OWC breakwater, and the wave force $F_{w,\text{Goda}}$ evaluated via Goda's model, for the selected records of Quasi-Standing Waves of Figs. 13 and 14.

Record	$F_{w,\max\_recorded}$ (kN/m)	$F_{w,\text{QD nolinear\_U-OWC}}$ (kN/m)	$F_{w,\text{Goda}}$ (kN/m)
136 corresponding to the first positive peak of the QSW wave force	7.53	6.89	9.31
264 corresponding to the second positive peak of the QSW wave force	4.96	4.88	6.26
258 corresponding to the third positive peak of the QSW wave force	4.51	4.79	7.29
165 corresponding to the fourth positive peak of the QSW wave force	5.51	5.21	7.69
60 corresponding to the fifth positive peak of the QSW wave force	6.95	6.53	8.49

the significant wave height H_{S_i} the maxima wave forces are recorded for decreasing values both of b_M and s_{u-duct}. Indeed, the extreme loads occur for the lowest range of b_M/L_{p0} , that is [0.14–0.28], when, for a fixed value of probability such as 1/1000 for instance, the dimensionless maximum positive peak force $F_{w,\max}/\sigma_{F_w}$ exceeds the threshold 5 for "Quasi-Standing Waves", 9 for "Slightly Breaking Waves" and 12–14 for "Impact Loads", respectively. Analogous trends are obtained for the lowest values of the ratio s_{U-duct}/L_{p0}, ranging in the interval [0.02–0.04].

Finally, in the lower panels of Fig. 12, the influence of the Ursell number is considered showing that the greatest positive peak forces occur for lower values of U_r, for every wave loading conditions. Note that, when the Ursell number decreases, the non-linearities are increased at a breakwater in terms of distortion of the shape profiles in the wave pressure time series with the occurrence of significant double peaks, and with the maximum nonlinear wave pressure comparable to that one of the linear profile (Romolo and Arena, 2013).

6. The time-domain QD nonlinear model for the U-OWC power plant: calculation of the wave forces on the modified breakwater for the case of "Quasi-Standing Waves"

Following the Boccotti's approach (2012, 2014), the wave pressure, $\overline{\Delta p}_{U-OWC}$, on the outer opening of the vertical U-duct breakwater deployed at the NOEL laboratory can be estimated.

In particular, we apply the first formulation of the Quasi-Determinism (QD) theory (Boccotti, 2012, 2014), which allows us to predict, with a probability approaching 1, the expected configuration of the random wave field in the time domain before and after a time instant t_0, and in the space domain in the area surrounding a fixed point $\underline{x}_0 \equiv (x_0, y_0)$ at any depth z, when a large value (positive or negative) h of the water elevation occurs at the point $\underline{x}_0$ at t_0 in a random sea state, which is assumed to be a stationary and Gaussian process in the time domain.

Under this hypothesis, the QD theory proves that when $h/\sigma \to \infty$ (where σ is the root mean square of the surface displacement at $\underline{x}_0$) the configuration of the linear water elevation tends, with a probability approaching 1, to a well-defined average feature in space and time. By considering the U-OWC breakwater, the linear deterministic solution for the free surface displacement at the location of the innovative structure, that is to say at $\underline{x}_0 \equiv (x_0, y_0) = 0$, in time domain yields to

$$\overline{\eta}^{(1)}_{U-OWC}(T) = \beta \frac{h}{\sigma^2} \int_0^{\infty} \int_0^{2\pi} S(\omega,\theta)\cos(\omega T)\mathrm{d}\theta\, \mathrm{d}\omega, \tag{25}$$

with the associated wave pressure at level z in time domain given by

$$\overline{\Delta p}^{(1)}_{U-OWC}(z,T) = \rho g \beta \frac{h}{\sigma^2} \int_0^{\infty} \int_0^{2\pi} S(\omega,\theta) \frac{\cosh[k(d+z)]}{\cosh(kd)} \cos(\omega T)\mathrm{d}\theta\, \mathrm{d}\omega, \tag{26}$$

with, ρ the water density, g is the acceleration due to gravity. Moreover, in Eqs. (25) and (26), $S(\omega,\theta)$ is the directional wave spectrum of the incident waves, and σ^2 is the variance of the surface displacement of the wind-generated wave field (which as a whole is assumed to be random, stationary, and Gaussian) which is given by

$$\sigma^2 = \int_0^{\infty} \int_0^{2\pi} S(\omega,\theta)\mathrm{d}\theta\, \mathrm{d}\omega, \tag{27}$$

where the wave frequency ω and wavenumber k both satisfy the linear dispersion rule

$$\omega^2 = gk\tanh(kd) \tag{28}$$

Finally, in the solutions both of the free surface displacement (Eq. (25)) and of the wave pressure (Eq, 26), the coefficient β is the so-called *amplification factor,* defined as the following ratio

$$\beta = \frac{\text{wave crest at the breakwater embodying the U} - \text{OWC}}{\text{wave crest at a conventional vertical breakwater}} \tag{29}$$

Thus, the coefficient β is equal to 1 for a conventional breakwater and it is for a U-OWC breakwater the lower than 1, the higher the energy absorption coefficient C_{abs} (Eq. (3)) of the U-OWC pneumatic chambers is.

Then, following the Romolo and Arena (2013) and Romolo et al. (2014) approaches, the second-order corrections both to the linear deterministic free surface displacement and to the first-order deterministic wave pressure at the U-OWC is determined.

In detail, the second-order component of the deterministic free surface displacement at the U-OWC breakwater in time domain, is given by

$$\overline{\eta}^{(2)}_{U-OWC}(T) = \frac{\beta^2 h^2}{8\sigma^4} \left\{ \int_0^{\infty} \int_0^{\infty} \int_0^{2\pi} \int_0^{2\pi} S(\omega_1,\theta_1)S(\omega_2,\theta_2) \left\{ \left(\mathrm{A}_1^- + \mathrm{A}_2^-\right)[\cos(\omega_1-\omega_2)T] + \left(\mathrm{A}_1^+ + \mathrm{A}_2^+\right)[\cos(\omega_1+\omega_2)T] + F(\omega_1,\omega_2,\theta_1,\theta_2)\right\} \mathrm{d}\theta_2\, \mathrm{d}\theta_1\, \mathrm{d}\omega_2\, \mathrm{d}\omega_1 \right. \tag{30}$$

and the second-order component of the deterministic wave pressure is found to be

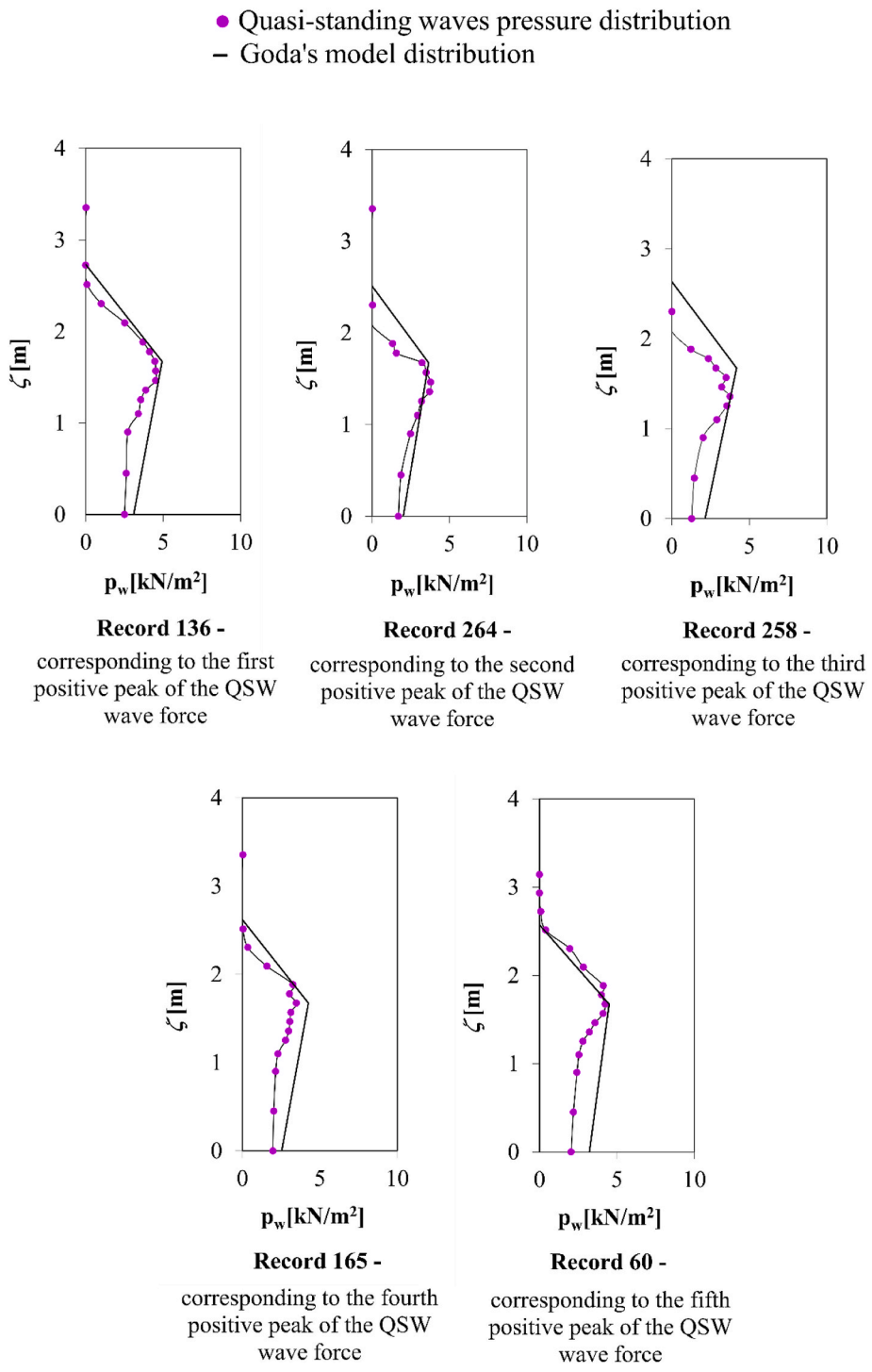

Fig. 14. Pressure distributions relative to the first 5 greatest positive force peaks $\widetilde{F}(t)$ for "Quasi Standing waves" versus Goda's model.

$$\overline{\Delta p}^{(2)}_{U-OWC}(z,T) = \rho g^2 \frac{\beta^2 h^2}{8\sigma^4} \left\{ \int_0^\infty \int_0^\infty \int_0^\infty \int_0^\infty S(\omega_1,\theta_1) S(\omega_2,\theta_2) \left\{ \omega_1^{-1}\omega_2^{-1}\left(C_1^- + C_2^-\right)[\cos(\omega_1-\omega_2)T] + \omega_1^{-1}\omega_2^{-1}\left(C_1^+ + C_2^+\right)[\cos(\omega_1+\omega_2)T] \right.\right.$$

$$\left.\left. + g^{-1}F(\omega_1,\omega_2,\theta_1,\theta_2) \right\} \mathrm{d}\theta_2 \mathrm{d}\theta_1 \mathrm{d}\omega_2 \mathrm{d}\omega_1 - 4\left[\int_0^\infty \int_0^{2\pi} S(\omega_1,\theta_1)\omega_1^{-1} k_1 \frac{\sinh[k_1(d+z)]}{\cosh(k_1 d)} \sin(\omega_1 T) \mathrm{d}\theta_1 \mathrm{d}\omega_1 \right]^2 \right\} \tag{31}$$

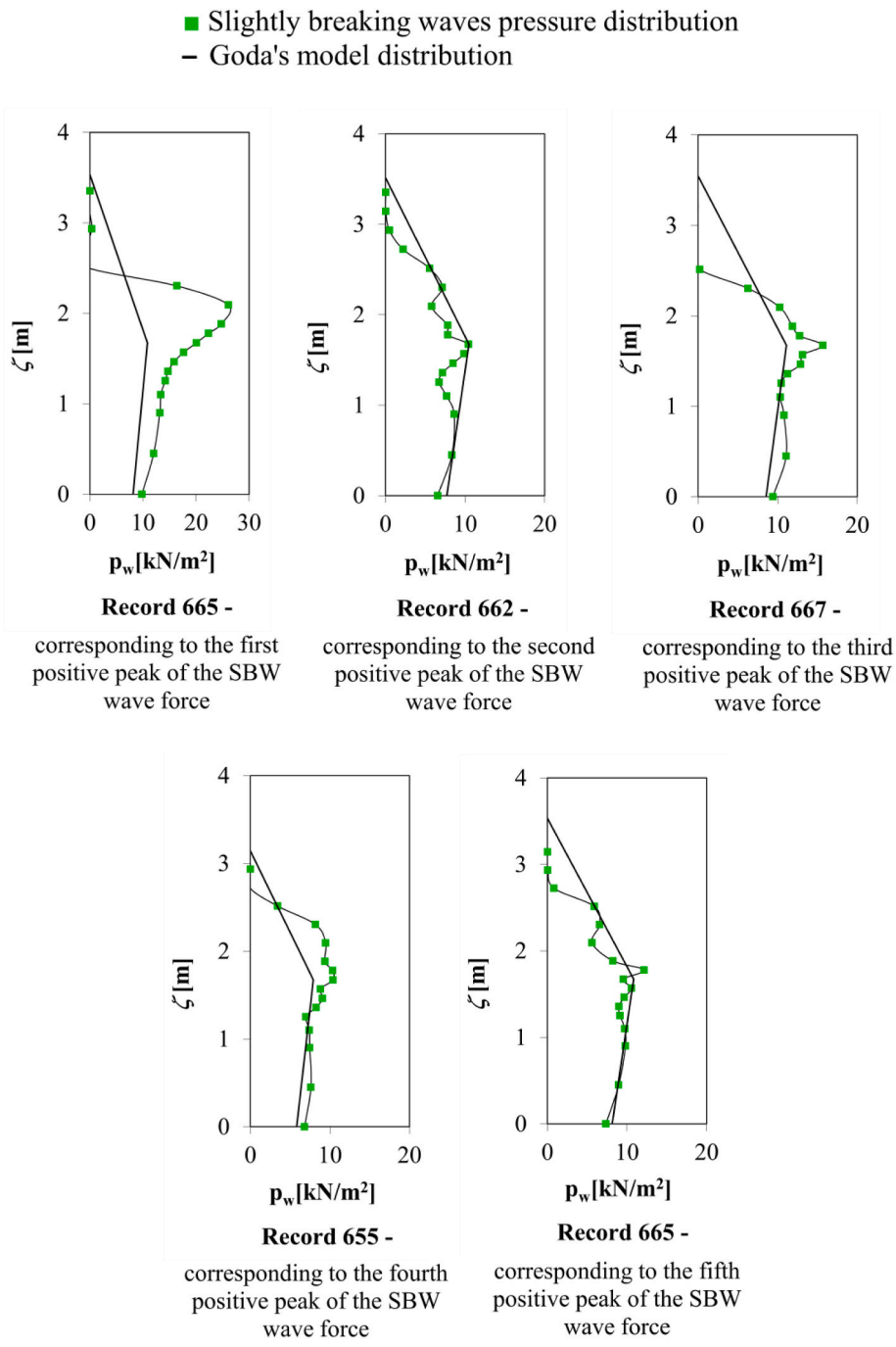

Fig. 15. Pressure distributions relative to the first 5 greatest positive force peaks $\widetilde{F}(t)$ for "Slightly Breaking waves" versus Goda's model.

where

$$F(\omega_1,\omega_2,\theta_1,\theta_2)=\begin{cases}\dfrac{2k_1}{\sinh(2k_1d)} & \text{if } \omega_1=\omega_2 \quad \text{and } \theta_1=\theta_2\\ 0 \quad \text{if } \omega_1\neq\omega_2 \quad \text{and } \theta_1\neq\theta_2\,.\end{cases} \tag{32}$$

The QD nonlinear theory for the U-OWC breakwater presented in the paper is tested by considering the experimental data and using as input in the theoretical computations the characteristic parameter values, that are the significant wave height, H_{S_i}, the peak period, T_p, and the β coefficient of Eq. (29) equal to those of the analysed record, and provided in Table 4. The dominant wave direction is orthogonal to the U-OWC breakwater in all the records. As for the theoretical directional spectrum, a Pierson Moskowitz-Mitsuyasu is assumed. For the selected five most intense records of Quasi-Standing wave, the related wave pressure distributions are provided in Fig. 13, where orange dots represent the measured wave pressures along depth and blue lines are the analytical results of the QD solution up to second-order at the U-OWC breakwater. From the bottom to the mean water level (mwl), the wave pressure is calculated by Eqs. (26) and (31):

$$\overline{\Delta p}_{U-OWC}(z,T)=\overline{\Delta p}^{(1)}_{U-OWC}(z,T)+\overline{\Delta p}^{(2)}_{U-OWC}(z,T) \tag{33}$$

Then, we assume a linear trend from the mwl to the maximum wave elevation evaluated via Eqs. (25) and (30)

$$\overline{\eta}_{U-OWC}(T)=\overline{\eta}^{(1)}_{U-OWC}(T)+\overline{\eta}^{(2)}_{U-OWC}(T) \tag{34}$$

By comparing the measured and the analytical wave pressure

Table 6
The recorded wave force $F_{w,\max\_recorded}$ acting on the U-OWC model and the wave force calculated via Goda's model $F_{w,Goda}$, for the selected records of Slightly Breaking Waves of Fig. 15.

Record	$F_{w,\max\_recorded}$ (kN/m)	$F_{w,Goda}$ (kN/m)
665 corresponding to the first positive peak of the SBW wave force	38.86	25.94
662 corresponding to the second positive peak of the SBW wave force	20.97	24.83
667 corresponding to the third positive peak of the SBW wave force	26.54	26.77
655 corresponding to the fourth positive peak of the SBW wave force	20.77	17.29
665 corresponding to the fifth positive peak of the SBW wave force	22.88	25.94

distributions of Fig. 13, an excellent agreement is observed. Moreover, the wave force is estimated by integrating the wave pressure along the depths. The results are provided in Table 5, showing that the wave forces predicted via the QD nonlinear model at the U-OWC breakwater differ by only 5–6 % from the measured values. It is, finally, observed that the QD nonlinear model has been achieved assuming the fluid to be incompressible and inviscid, and the flow irrotational. Therefore, the QD nonlinear model can applied only to the case of Quasi-Standing wave pattern, in the absence of an impulsive breaking component.

7. The Goda's model applied for evaluation of wave pressure on the U-OWC breakwater

ln literature the Goda's scheme (2000) is one of the most effective model, widely adopted to determine the pressure distribution on a seawall or a vertical breakwater, in the case either of breaking or non-breaking incident sea waves.

Goda's formulae are here applied to calculate the pressure distributions on the breakwater modified with the U-OWC technology, for the three considered conditions. Note that the Goda's approach has been applied also for OWC breakwater by Pawitan et al. (2019), for the calculation of wave pressures both on the external wall and internal walls of the pneumatic chamber. In the present study, we assume, in the Goda's model, the design wave height H equal to $1.8H_{S_i}$, where H_{S_i} is the significant height of the incident waves calculated via the time series data of the free surface displacement obtained from the two ultrasonic probes in the undisturbed wave field (see Section 1). Moreover, the wave period T of the design wave is assumed equal to the zero up-crossing period of the central wave of wave groups, T_h, according to the Quasi-Determinism theory (Boccotti, 2000). In particular, for pure wind waves, assuming a mean JONSWAP frequency spectrum, the T_h wave period is assumed equal to 0.92 T_p, T_p being the peak period of incoming waves.

In Figs. 14 and 15, the comparison between the experimental wave pressure distributions and the theoretical distributions calculated using Goda's model are shown, for the cases both of "Quasi Standing (QS) waves" and "Slightly Breaking (SB) waves", respectively. In details, the 5 highest positive peaks of wave force related to loading conditions of "Quasi Standing waves" and "Slightly Breaking waves" are identified, and the relative measured wave pressure distributions are shown (see dots purple in Fig. 14 for QS waves and dots green in Fig. 15 for SB waves). Then, the theoretical wave pressure distributions are calculated via Goda's model, defined in Appendix B. The results are reported in Figs. 14 and 15 as continuous lines in both graphs. The comparison of the recorded and the theoretical trends shows an overall good agreement, especially below the mean water level. Then, for the selected cases reported in Figs. 14 and 15, the wave force corresponding to the considered wave pressure distribution, is calculated. The values of QS waves are given in Table 5, and those of SB waves are reported in Table 6. A comparison between recorded experimental wave force $F_{w,\max\_recorded}$ acting on the U-OWC model and wave force calculated via

Table 7
The recorded wave force $F_{w,\max\_recorded}$ acting on the U-OWC model and the wave force calculated via Goda's model $F_{w,Goda}$, for the selected records of Impact Loads of Fig. 16.

Record	$F_{w,\max\_recorded}$ (kN/m)	$F_{w,Goda}$ (kN/m)
669 corresponding to the first positive peak of the IL wave force	42.37	24.26
667 corresponding to the second positive peak of the IL wave force	36.29	26.77
664 corresponding to the third positive peak of the IL wave force	28.59	20.08

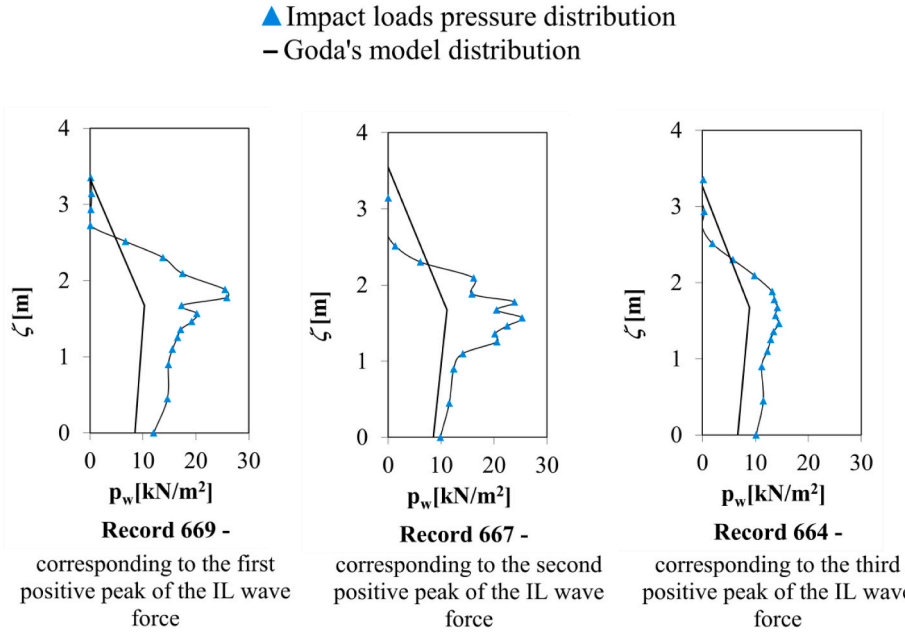

Fig. 16. Pressure distributions relative to the first 3 greatest positive force peaks $\widetilde{F}(t)$ for "Impact Loads" versus Goda's model.

Goda's model $F_{w,\mathrm{Goda}}$ shows as the Goda's approach tends to overestimate between 25 and 60 percent the measured values for the loading case of QS waves (Table 5), while a better agreement is observed with the data in the case of SB waves (Table 6), when the differences are among 17 and 30 %.

Finally, the same procedure is applied for the case of Impact Loads. Fig. 16 represents the recorded wave pressure distributions (dots light blue in Fig. 16) of the 3 greatest positive peaks of the force process $\widetilde{F}(t)$ for the class of impact loads. Then, the Goda's formulae are applied to calculate the theoretical pressure distributions for the selected records of Fig. 16 (continuous line). In all three records, the theoretical Goda's scheme underestimates significantly, by 25–40 %, the impulsive force obtained by the experimental pressure distributions. These results are given in Table 7.

Therefore, the experimental wave pressure distributions show as the existing Goda's approach revels important limitations to predict impulsive pressures and forces on the U-OWC model for the cases both of "Quasi-Standing" waves and "Impact loads", while this theoretical scheme is in quite well in agreement with experimental results of "Slightly Breaking" waves.

8. Conclusions

In this paper, the analysis of the wave pressures and the wave loads acting on the modified U-OWC breakwater during field experiment in the NOEL laboratory is pursued.

Moreover, the hydrodynamics inside the active parts of the U-OWC device for the exploitation of wave energy and incorporated into a caisson breakwater is calculated. The U-OWC plant proves to have high energetic performances in terms of absorption of incident wave energy, even during sea states with violent wave loads. A global force is realized in the U-duct and the inner pneumatic chamber, which proves to increase the overall stability of the structure. Thus, it can be neglected for the sake of the structure safety.

Thus, the evaluation of horizontal force due to sea waves is fundamental, since it is the only ones that can produce instability of the U-OWC breakwater. In details, the post processing of the small-scale experiment reveals the occurrence of both pulsating (quasi-static) wave forces and impact wave loads. In particular, three wave loading conditions are identified; these are "Quasi-Standing (QS)", "Slightly Breaking (SB)", "Impact Loads (IL)". Wave pressure distributions and wave forces are evaluated for all loading conditions, showing that impulsive waves (IL) can produce maximum pressures and positive peaks of wave loads greater than up to 5 times those recorded for quasi-standing conditions.

Then, a parametric analysis with a probabilistic approach is developed to investigate the influence of the U-OWC structure geometry, the seabed topography in front and in the proximity of the modified breakwater, the wave steepness, the spectrum of incoming waves, the non-linearities, on the occurrence of wave impact loads. It is shown that the most critical conditions, associated to the most severe wave loads on the modified U-OWC breakwater, are realized for deeper water depths d_n given a fixed significant wave height H_{S_i} in the case of "Quasi-Standing" waves. Instead, for "Slightly Breaking waves"; and "Impact Loads", the extreme loads are recorded for the most intense sea states, with greater H_{S_i} , and for decreasing values of the water depth d_n. In these cases, the recorded peaks of extreme loads positive force peaks are about to $14 - 16\sigma_{F_w}$ (σ_{F_w} being the standard deviation of the recorded wave force). The same trends are observed for decreasing depth, d'. in front of the breakwater and. when the depth, a , of the U-opening is significantly reduced, producing breaking waves at the modified breakwater. Moreover, positive force peaks equal to $12 - 14\sigma_{F_w}$ are recorded either for lower widths of the berm b_M and of the U-duct s_{u-duct}.

This analysis in term of probability of exceedance turns out to be useful in the preliminary design stage of the U-OWC breakwater, to properly sizing the structural elements of the structure in order to avoid extreme and violent wave loads acting on it.

Finally, two different models are validated against the field data recorded at the U-OWC model of the NOEL laboratory.

The first model is the analytical Quasi-Determinism (QD) nonlinear model in time domain at the U-OWC breakwater, which is valid for an incompressible and inviscid fluid, and for an irrotational flow. Thus, it can be applied only for wave forces due to Quasi-Standing wave conditions. It proves to have an excellent agreement with experimental field data, and, thus, it can be properly applied for the estimation of wave forces at the U-OWC breakwater due to sea waves, in the absence of impulsive loads.

The second model considered is the Goda's model, which was considered to calculate the wave pressure distributions on the external walls of the U-OWC breakwater for the three wave load conditions identified. It is observed that the Goda's formulae applied to U-OWC are in good agreement with the data in the case of "Slightly Breaking (SB)" wave loads, while they tend to overestimate experimental results for "Quasi-Standing (QS)" waves and, to significantly, underestimate "Impact Load (IL)" conditions. Therefore, the model can be suitable applied for the estimate of the overall stability of the U-OWC breakwater for the case of SBW, being conservative.

Following the approach developed in the present paper, when the wave force is determined on a U-OWC breakwater, the wave load behaviour can be identified assuming either a "Quasi-Standing (QS)", or a "Slightly Breaking (SB)", or an "Impact Load (IL)" wave. Otherwise, for a fixed geometry both of the U-OWC device and of the depths in front of the structure, it is also possible to predict the most probable wave load condition that can occur on the modified structure. Consequently, the proper model for the estimation of wave pressure distribution acting on the structure can be adopted for the evaluation of the global stability of the structure. In the case of QSWs, the non-linear QD analytical model can be suitable adopted assuring effective results and predictions. When a SBW force occurs, Goda's formulae applied to the U-OWC can be conveniently applied for a safe design, providing a limited overestimate of the expected wave loads. Finally, both models show some limitations in the predictions of the expected wave loads in the case of ILs.

CRediT authorship contribution statement

Alessandra Romolo: Conceptualization, Formal analysis, Investigation, Methodology, Software, Supervision, Validation, Visualization, Writing – original draft, Writing – review & editing. **Bruna Timpano:** Conceptualization, Formal analysis, Investigation, Methodology, Software, Validation, Visualization, Writing – original draft, Writing – review & editing. **Valentina Laface:** Conceptualization, Investigation, Software, Visualization, Writing – original draft, Writing – review & editing. **Vincenzo Fiamma:** Data curation, Investigation, Resources, Visualization, Writing – review & editing. **Felice Arena:** Conceptualization, Data curation, Funding acquisition, Project administration, Resources, Supervision, Validation, Writing – review & editing.

Declaration of competing interest

The authors declare that they have no known competing financial interests or personal relationships that could have appeared to influence the work reported in this paper.

Data availability

Data will be made available on request.

Acknowledgement

The paper has been partially supported by Project "Green Campania Ports - Port of Salerno", by "Asse D - Green Ports" of PAC Infrastructures

and Networks 2014-2020, Italian Ministry of Infrastructures.

Appendix A. The interaction kernels of the second-order deterministic components both of the surface displacement and of the wave pressure for the wave field in front of the U-OWC breakwater

The interaction kernels of the nonlinear free-surface displacement are given by

$$\begin{aligned}&A_n^-(\omega_1,\omega_2,\theta_1,\theta_2;d) = g\omega_1^{-1}\omega_2^{-1}\left\{B_n^- - k_1k_2[-(-1)^n\cos(\theta_1+(-1)^n\theta_2)+\tanh(k_1d)\tanh(k_2d)]\right\}+\left(\omega_1^2+\omega_2^2\right)/g^2\\ &n=1,2\\ &A_n^+(\omega_1,\omega_2,\theta_1,\theta_2;d) = g\omega_1^{-1}\omega_2^{-1}\left\{B_n^+ - k_1k_2[-(-1)^n\cos(\theta_1+(-1)^n\theta_2)-\tanh(k_1d)\tanh(k_2d)]\right\}+\left(\omega_1^2+\omega_2^2\right)/g^2\end{aligned} \tag{A1}$$

with coefficients $B_n^{\mp}$ ($n = 1,2$) expressed by

$$\begin{aligned}&B_n^-(\omega_1,\omega_2,\theta_1,\theta_2;d) = -\frac{\Lambda_n^-\omega_1\omega_2(\omega_1-\omega_2)/g^2}{(\omega_1-\omega_2)^2 - g|\underline{\mathbf{k}}_n^-|\tanh\left(|\underline{\mathbf{k}}_n^-|d\right)} \quad n=1,2\\ &B_n^+(\omega_1,\omega_2,\theta_1,\theta_2;d) = -\frac{\Lambda_n^+\omega_1\omega_2(\omega_1+\omega_2)/g^2}{(\omega_1+\omega_2)^2 - g|\underline{\mathbf{k}}_n^+|\tanh\left(|\underline{\mathbf{k}}_n^+|d\right)}\end{aligned} \tag{A2}$$

$\Lambda_n^{\mp}$ ($n = 1,2$) coefficients and wave numbers $\underline{\mathbf{k}}_n^{\mp}$ ($n = 1,2$) being, respectively

$$\begin{aligned}&\Lambda_n^-(\omega_1,\omega_2,\theta_1,\theta_2;d) = -\frac{\omega_1^3}{\sinh^2(k_1d)}+\frac{\omega_2^3}{\sinh^2(k_2d)}-2\omega_1\omega_2(\omega_1-\omega_2)-(-1)^n2g^2\left(\omega_1^{-1}-\omega_2^{-1}\right)k_1k_2\cos[\theta_1+(-1)^n\theta_2]\\ &n=1,2\\ &\Lambda_n^+(\omega_1,\omega_2,\theta_1,\theta_2;d) = -\frac{\omega_1^3}{\sinh^2(k_1d)}-\frac{\omega_2^3}{\sinh^2(k_2d)}+2\omega_1\omega_2(\omega_1+\omega_2)+(-1)^n2g^2\left(\omega_1^{-1}+\omega_2^{-1}\right)k_1k_2\cos[\theta_1+(-1)^n\theta_2]\end{aligned} \tag{A3}$$

$$\begin{aligned}&\underline{\mathbf{k}}_n^-(\omega_1,\omega_2,\theta_1,\theta_2) = \left(k_1\sin\theta_1 - k_2\sin\theta_2;\ \ k_1\cos\theta_1+(-1)^nk_2\sin\theta_2\right) \quad n=1,2\\ &\underline{\mathbf{k}}_n^+(\omega_1,\omega_2,\theta_1,\theta_2) = \left(k_1\sin\theta_1 + k_2\sin\theta_2;\ \ k_1\cos\theta_1-(-1)^nk_2\sin\theta_2\right)\end{aligned} \tag{A4}$$

Finally, the interaction kernels of the wave pressure up to second-order are expressed by

$$\begin{aligned}&C_n^-(\omega_1,\omega_2,\theta_1,\theta_2) = B_n^-\frac{\cosh\left[|\underline{\mathbf{k}}_n^-|(d+z)\right]}{\cosh\left(|\underline{\mathbf{k}}_n^-|d\right)}\\ &C_n^+(\omega_1,\omega_2,\theta_1,\theta_2) = B_n^+\frac{\cosh\left[|\underline{\mathbf{k}}_n^+|(d+z)\right]}{\cosh\left(|\underline{\mathbf{k}}_n^+|d\right)}.\end{aligned} \quad n=1,2 \tag{A5}$$

where the $B_n^{\mp}$ ($n = 1,2$) coefficients are expressed by Eq. (A2) and $\underline{\mathbf{k}}_n^{\mp}$ ($n = 1,2$) are the vectors of wave numbers for the three-dimensional solution.

Assuming that the sea waves approach orthogonally to the U-OWC breakwater, the direction of propagations θ_n ($n = 1,2$) with respect to the normal to the breakwaters are null.

Appendix B. The Goda's model applied to the U-OWC breakwater deployed at the NOEL laboratory

In the present study, the Goda's model (2000) is applied with reference to the configuration of the U-OWC breakwater tested during the small-scale field experiment campaign arranged at NOEL laboratory (see Figs. 1 and 2).

The model for the pressure distribution proposed by Goda, is shown in Figure B1 and it provides the maximum elevation of the free surface, η_{max}, which is equal to

$$\eta_{max} = \frac{3}{4}(1+\cos\theta)H \tag{B1}$$

and the maximum (positive) wave pressures under a wave crest, which are given, with reference to the scheme of Fig. 2, by

$$p_{w1}^{(+)} = \frac{1}{2}(1+\cos\theta)\left(\alpha^I+\alpha^{II}\cos^2\theta\right)\gamma H \tag{B2}$$

$$p_w^{(+)} = \alpha^{III}p_{w1}^{(+)} \tag{B3}$$

$$p_{w2}^{(+)} = \left(1-\frac{h_M}{\eta_{max}}\right)p_{w1}^{(+)} \tag{B4}$$

$$p_{w3}^{(+)} = \left(1-\alpha^{IV}\right)p_{w1}^{(+)}+\alpha^{IV}p_w^{(+)} \tag{B5}$$

where γ is the water density, h_M is the quote of the top of U-OWC pneumatic chamber with respect to the mean water level (see Fig. 2), H is the height of the largest wave in the design sea state (see Section 6) and θ is the dominant direction of propagation of incoming waves with respect to the orthogonal to the U-OWC breakwater. In details, when the irregular sea waves approach orthogonally to U-OWC caissons, θ is equal to 0.

Moreover, in Equations (B2)-(B5), the coefficients α^I, α^{II}, α^{III} and α^{IV} are empirical and they are defined by the Goda's model (2000) as follows

$$\alpha^{I} = 0.6 + \frac{1}{2}\left[\frac{2kd_n}{\sinh(2kd_n)}\right]^2 \tag{B6}$$

$$\alpha^{II} = Min\left[\left(\frac{d_n^{'} - d^{'}}{3d_n^{'}}\right)\left(\frac{H}{d^{'}}\right)^2, 2\frac{d^{'}}{H}\right] \tag{B7}$$

$$\alpha^{III} = 1 - \frac{d}{d_n}\left[1 - \frac{1}{\cosh(kd_n)}\right] \tag{B8}$$

$$\alpha^{IV} = \frac{a}{d^{'}} \tag{B9}$$

where k is the wave number relative to the water depth d_n and the wave period of the design wave (see Section 6), with the associated wave length L. Then, d, $d^{'}$ and d_n are the water depths illustrated in Figure B1, while $d_n^{'}$ is defined as the water depth of the natural bed at a distance of $5H_{S_i}$ from the U-OWC breakwater.

Following the Goda's model (2000), the wave pressure $p_{w1}^{(+)}$ on the mean water level, is expressed by equation (B2) for the case of non-breaking waves, that is identified by conditions that

$$\frac{d_n}{H_{s_i}} \geq 2.4 \text{ and } \frac{d_n}{L} \geq 0.12 \tag{B10}$$

If relations (B10) are not satisfied, it is necessary to take into account an additional impulsive wave pressure contribution. In this case, the wave pressure $p_{w1}^{(+)}$ is defined by Goda (2000) by the following expression

$$p_{w1}^{(+)} = \frac{1}{2}(1 + \cos\theta)\left(\alpha^{I} + \alpha * \cos^2\theta\right)\gamma H \tag{B11}$$

where

$$\alpha * = Max\left\{\alpha^{II}, \alpha_I\right\} \tag{B12}$$

with α^{II} expressed by Eq. (B7) and coefficient α_I calculated by relation that

$$\alpha_I = \alpha_{IH}\alpha_{IB} \tag{B13}$$

being

$$\alpha_{IH} = \min\left\{\frac{H}{d^{'}};\ 2.0\right\} \tag{B14}$$

$$\alpha_{IB} = \begin{cases} \dfrac{\cos\delta_2}{\cosh\delta_1} : \delta_2 \leq 0, \\ \dfrac{1}{\cosh\delta_1 \cosh^{1/2}\delta_2} : \delta_2 > 0, \end{cases} \tag{B15}$$

$$\delta_1 = \begin{cases} 20\,\delta_{11} : \delta_{11} \leq 0, \\ 15\,\delta_{11} : \delta_{11} > 0, \end{cases} \tag{B16}$$

$$\delta_2 = \begin{cases} 4.9\,\delta_{22} : \delta_{22} \leq 0, \\ 3.0\,\delta_{22} : \delta_{22} > 0, \end{cases} \tag{B17}$$

$$\delta_{11} = 0.93\left(\frac{b_M}{L} - 0.12\right) + 0.36\left(0.4 - \frac{d^{'}}{d_n}\right), \tag{B18}$$

$$\delta_{22} = -0.36\left(\frac{b_M}{L} - 0.12\right) + 0.93\left(0.4 - \frac{d^{'}}{d_n}\right) \tag{B19}$$

In Eqs. (B18) and (B19), b_M is the length between the base of the U-OWC breakwater and the head of the foundation berm. L is the wave length at water depth d_n .

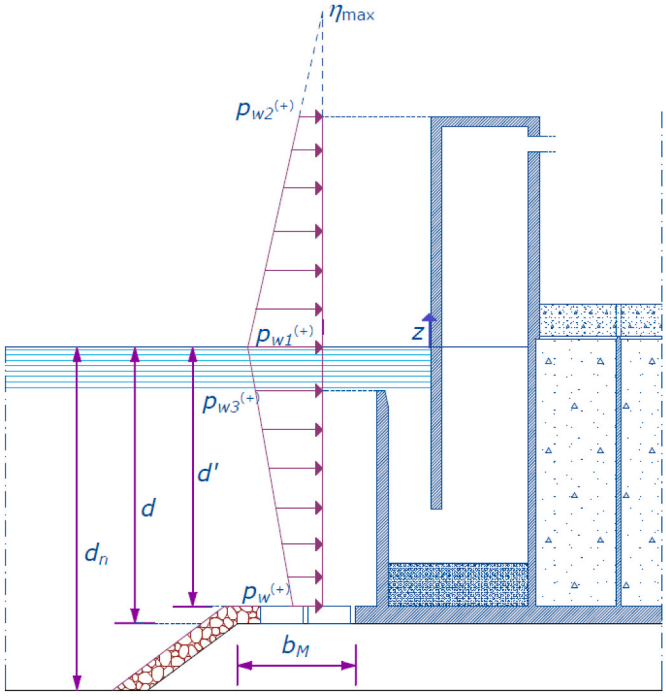

Figure B1. Scheme of Goda's model applied to U-OWC breakwater.

References

Arena and Pavone, 2006. The return period of non-linear high wave crests. J. Geophys. Res. https://doi.org/10.1029/2005JC003407.

Arena, F., Laface, V., Malara, G., Romolo, A., Viviano, A., Fiamma, V., Sannino, G., Carillo, A., 2015. Wave climate analysis for the design of wave energy harvesters in the Mediterranean Sea. Renew. Energy 77 (0), 125–141.

Arena, F., Romolo, A., Malara, G., Fiamma, V., Laface, V., 2018. "Response of the U-OWC Prototype Installed in the Civitavecchia Harbour," Proc of 37th International Conference of Offshore. Mechanics and Arctic Engineering, Madrid, Spain. OMAE2018-78762.

Bagnold, R.A., 1939. Interim Report on Wave-Pressure Research. Institution of Civil Engineeris. Technical Report.

Boccotti, P., 2000. Wave Mechanics for Ocean Engineering. Elsevier Science, Oxford, UK.

Boccotti, P., 2012. Design of breakwater for conversion of wave energy into electrical energy. Ocean. Eng. 51, 106–118. https://doi.org/10.1016/j.oceaneng.2012.05.011.

Boccotti, P., 2014. Wave Mechanics and Wave Loads on Marine Structures. Elsevier Science, Oxford, UK.

Boccotti, P., Filianoti, P., Fiamma, V., Arena, F., 2007. Caisson breakwaters embodying an OWC with a small opening-Part II: a small-scale field experiment. Ocean. Eng. 34 (5–6), 820–841.

Boccotti, P., Arena, F., Fiamma, V., Romolo, A., Barbaro, G., 2012. A small scale field experiment on wave forces on upright breakwaters. J. Waterw. Port, Coast. Ocean Eng.-ASCE 138, 97–114. https://doi.org/10.1061/(ASCE)WW.1943-5460.0000111.

Bullock, G., Crawford, A., Hewson, P., Walkden, M., Bird, P., 2001. The influence of air and scale on wave impact pressures. Coast. Eng. 42, 291–312.

Chen, X., Hofland, B., Molenaar, W., Capel, A., Van Gent, M.R.A., 2019. Use of impulses to determine the reaction force of a hydraulic structure with an overhang due to wave impact. Coast. Eng. 147, 75–88.

Cooker, M.J., Peregrine, D.H., 1995. Pressure impulse theory for liquid impact problems. J. Fluid Mech. 297, 193–214.

Cuomo, G., Allsop, W., Bruce, T., Pearson, J., 2010. Breaking wave loads at vertical seawalls and breakwaters. Coast. Eng. 57, 424–439.

Goda, Y., 2000. Random Seas and Design of Maritime Structures. Advanced Series on Ocean Engineering. World Scientific, Singapore.

Hasselmann, K., Barnett, T.P., Bouws, E., Carlson, H., Cartwright, D.E., Eake, K., Euring, J.A., Gicnapp, A., Hasselmann, D.E., Kruseman, P., Meerburg, A., Mullen, P., Olbers, D.J., Richren, K., Sell, W., Walden, H., 1973. Measurements of wind-wave growth and swell decay during the joint North Sea wave project (JONSWAP). Ergänzungsheft zur Deutschen Hydrographischen Zeitschrift A8 (Nr. 12), 1–95.

Kirkgoz, M.S., 1982. Shock pressure of breaking waves on vertical walls. J. Waterw. Port, Coast. Ocean Eng.-ASCE 108, 81–95.

Oumeraci, H., Klammer, P., Partenscky, H., 1993. Classification of breaking wave loads on vertical structures. J. Waterw. Port, Coast. Ocean Eng.-ASCE 119, 381–397.

Oumeraci, H., Kortenhaus, A., Allsop, W., de Groot, M., Crouch, M., Vrijling, H., Voortman, H., 2001. Probabilistic Design Tools for Vertical Breakwaters. Balkema, Lisse, p. 373.

Pawitan, K.A., Dimakopoulos, A.S., Vicinanza, D., Allsop, W., Bruce, T., 2019. A loading model for an OWC caisson based upon large-scale measurements. Coast. Eng. 145, 1–20.

Peregrine, D.H., 2003. Water-wave impact on walls. Annu. Rev. Fluid Mech. 35, 23–43. https://doi.org/10.1146/annurev.fluid.35.101101.161153.

Pierson, W.J., Moskowitz, L.A., 1964. A proposed spectral form for fully developed waves based on the similarity theory of S. A. Kitaigorodskii. J. Geophys. Res. 69, 5181–5190.

Romolo, A., Arena, F., 2008. Mechanics of nonlinear random wave groups interacting with a vertical wall. Phys. Fluids 20 (3). https://doi.org/10.1063/1.2890474, 036604-1-036604-16.

Romolo, A., Arena, F., 2013. Three-dimensional non-linear standing wave groups: Formal derivation and experimental verification. Int. J. Non Lin. Mech. https://doi.org/10.1016/j.ijnonlinmec.2013.08.005.

Romolo, A., Arena, F., Laface, V., 2014. A generalized approach to the mechanics of three-dimensional nonlinear ocean waves. Probabilist. Eng. Mech. 35, 96–107. https://doi.org/10.1016/j.probengmech.2013.10.009.

Viviano, A., Musumeci, R.E., Vicinanza, D., Foti, E., 2019. Pressures induced by regular waves on a large scale OWC. Coast. Eng. 152, 103528.

Wood, D.J., Peregrine, D.H., Bruce, T., 2000. Wave impact on a wall using pressure impulse theory. I: trapped air. J. Waterw. Port, Coast. Ocean Eng-ASCE. 126, 182–190.

Zhao, X., Zou, Q., Geng, J., Zhang, Y., Wang, Z., 2022. Influences of wave resonance on hydrodynamic efficiency and loading of an OWC array under oblique waves. Appl. Ocean Res. 120, 103069.